

What limits predictive certainty of long term carbon uptake?

B. Raczka, S. Serbin

To be published in "Journal of Geophysical Research: Biogeosciences"

November 2018

Environmental and Climate Sciences Department
Brookhaven National Laboratory

U.S. Department of Energy

USDOE Office of Science (SC), Biological and Environmental Research (BER) (SC-23)

Notice: This manuscript has been authored by employees of Brookhaven Science Associates, LLC under Contract No. DE-SC0012704 with the U.S. Department of Energy. The publisher by accepting the manuscript for publication acknowledges that the United States Government retains a non-exclusive, paid-up, irrevocable, world-wide license to publish or reproduce the published form of this manuscript, or allow others to do so, for United States Government purposes.

DISCLAIMER

This report was prepared as an account of work sponsored by an agency of the United States Government. Neither the United States Government nor any agency thereof, nor any of their employees, nor any of their contractors, subcontractors, or their employees, makes any warranty, express or implied, or assumes any legal liability or responsibility for the accuracy, completeness, or any third party's use or the results of such use of any information, apparatus, product, or process disclosed, or represents that its use would not infringe privately owned rights. Reference herein to any specific commercial product, process, or service by trade name, trademark, manufacturer, or otherwise, does not necessarily constitute or imply its endorsement, recommendation, or favoring by the United States Government or any agency thereof or its contractors or subcontractors. The views and opinions of authors expressed herein do not necessarily state or reflect those of the United States Government or any agency thereof.

1 **What limits predictive certainty of long term carbon uptake?**
2 **Quantifying parametric uncertainty at a site in Northern**
3 **Wisconsin**

4 **Brett Raczka^{1*}, Michael C. Dietze², Shawn P. Serbin³, Kenneth J. Davis¹**

5 [1]{Dept. of Meteorology & Atmospheric Science, Pennsylvania State University, University
6 Park, Pennsylvania}

7 [2]{Dept. of Earth & Environment, Boston University, Boston, Massachusetts}

8 [3]{Environmental and Climate Sciences Department, Brookhaven National Laboratory, Upton,
9 NY, USA}

10

11 Correspondence to: B. Raczka (brett.raczka@utah.edu)

12 * Corresponding author is currently at Department of Biology, University of Utah, Salt Lake
13 City, Utah

14

15 **Key Points:**

- 16
- 17 • Parametric uncertainty from quantum efficiency and leaf respiration rate contributed most to model output uncertainty
 - 18 • Uncertainty from empirical water conductance and growth respiration parameters should be reduced with better model process representation
 - 19 • The inclusion of parameter random effects (across-site trait variation) changes the relative parametric contributions to model output uncertainty
- 20
21
22

23

24

25

26

27

28 **Abstract**

29 Terrestrial biosphere models can help identify physical processes that control carbon dynamics,
30 including land-atmosphere CO₂ fluxes, and have the potential to project the terrestrial ecosystem
31 response to changing climate. Observations are critical to evaluate model performance and to
32 guide improvements to the representation of ecological processes within the models. Here we
33 identify model parameters that contribute the most uncertainty to long term (~100 years)
34 projections of net ecosystem exchange (NEE), net primary production (NPP) and above ground
35 biomass (AGB) within a mechanistically detailed model (Ecosystem Demography, version 2.1).
36 Through an uncertainty analysis that constrains parameters using observations of plant traits and
37 site observations of NEE and AGB, we find quantum efficiency and leaf respiration rate
38 parameters as the highest contributors to model uncertainty regardless of time frame (annual,
39 decadal, centennial) and predictive variable (e.g. NEE, NPP, AGB). Key actions for model
40 improvement include additional measurements of quantum efficiency and leaf respiration rate,
41 both of which can be observed directly at the leaf level. We caution that the order in which
42 parameters contributed to model uncertainty was sensitive to the inclusion of parameter random
43 effects (across-site variation) in the analysis. Our finding was dependent upon the availability of
44 site-to-site trait observations and whether to account for that variability within the parameter
45 uncertainty. This analysis focused on parametric uncertainty; including contributions from initial
46 conditions, meteorological driver data and process error in future studies will provide a more
47 complete picture of the sources of uncertainty and observations needed to improve long-term
48 predictions.

49

50 **1 Introduction**

51 The response of the terrestrial biosphere to a changing climate remains a significant
52 uncertainty to climate prediction [Arora *et al.*, 2013; Friedlingstein *et al.*, 2014]. Climate
53 prediction relies in part upon terrestrial biosphere models (TBMs) that simulate fluxes and pools
54 of thermal energy, water, carbon, and momentum between the land-atmosphere interface.
55 Although TBM uncertainty stems from several sources including model parameters, initial
56 conditions (e.g. soil and vegetation state), and model driver data (e.g. meteorological conditions),
57 it has been demonstrated that biospheric model parameters are one of the most significant
58 contributors to TBM simulation uncertainty [Lin *et al.*, 2011].

59 Ecosystem observations improve TBM performance by optimizing the parameter values to
60 match ecosystem behavior [e.g. *Dietze et al.*, 2013]. These observations include chamber gas-
61 exchange measurements, eddy covariance flux measurements (carbon, sensible, and latent heat
62 flux) [e.g. *Braswell et al.*, 2005], above and below-ground biomass [e.g. *Medvigy et al.*, 2009],
63 leaf area and chemistry, and information on soil properties. Through the use of remote sensing
64 data, many of these critical measurements for informing models are obtained regionally using
65 active and passive remote sensing systems [*Schimel et al.*, 2015; *Shugart et al.*, 2015]. The
66 importance of constraining model parameters with data is supported by the relative high
67 performance of simple models (e.g. LOTEC, EC-MOD) used within a data assimilation
68 framework [*Keenan et al.*, 2012; *Raczka et al.*, 2013]. More recent studies have incorporated the
69 biometric observation of annual woody increment, or carbon stocks, which has shown the
70 capacity to constrain inter-annual to decadal processes (i.e. 5-20 years) when compared to
71 observations of carbon fluxes alone [*Ricciuto et al.*, 2011; *Richardson et al.*, 2010]. Despite the
72 power of data assimilation for informing models with data directly, *Weng and Luo*, [2011]
73 showed that 10 years of observations (e.g. biomass pools, soil carbon pools, soil respiration)
74 assimilated into a TBM at the Duke FACE experiment only reduced forecasting uncertainty for a
75 few decades; century-scale carbon cycle forecasts were not well-constrained. Overall, relatively
76 short term (<20 years) eddy covariance flux measurements of net ecosystem exchange (NEE)
77 reduce uncertainty at the sub-daily to seasonal time frames, but not inter-annual variations in net
78 carbon exchange and storage [*Braswell et al.*, 2005; *Ricciuto et al.*, 2008]. In general, TBM's
79 have difficulty capturing inter-annual variation in carbon uptake observed at flux towers with or
80 without data assimilation [*Keenan et al.*, 2012; *Raczka et al.*, 2013] and this could be a symptom
81 of inaccurate parameters or poorly represented ecological processes.

82 It is important to identify whether poorly represented processes at inter-annual time scales
83 also impact longer-term carbon dynamics (e.g. decadal to centennial time scales) because this
84 will have a large impact on future atmospheric CO₂ concentration and climate [*Arora et al.*,
85 2013; *Friedlingstein et al.*, 2014] . To design future experiments and observation systems that
86 can reduce model uncertainty, especially for centennial time scale predictions, the portion of a
87 TBM that contributes most to the uncertainty needs to be identified. This requires a TBM that
88 can capture the long-term ecosystem processes that control carbon balance.

89 The Ecosystem Demography Model [ED2; *Medvigy et al.*, 2009] simulates processes that
90 govern trends in the exchange of carbon between the atmosphere and terrestrial biosphere at
91 centennial time scales. ED2 uses size- and age-structured vegetation dynamics to capture the
92 competition that a single tree experiences for light, nutrients, and other resources.
93 Representation of this fine-scale competition is important for properly simulating successional
94 growth and long term carbon dynamics within a forest [*Pacala and Deutschman*, 1995], yet is
95 unaccounted for in the more common ‘big-leaf’ TBMs [*Levin et al.*, 1997]. Although tracking
96 size structure to capture fine-scale dynamics of plants is not unique to ED2 [*Fisher et al.*, 2018]],
97 ED2’s methodology for tracking the landscape-scale distribution of the size-age class
98 distribution allows for the efficient spatial scaling from the cohort to patch to regional scales.
99 Compared to other TBMs ED2 has a mechanistically-detailed representation of plant
100 ecophysiology, photosynthesis, tree demography, soil biogeochemistry and hydrology, as well as
101 biophysical fluxes of surface energy, moisture, and momentum [*Medvigy et al.*, 2009; *Rogers et*
102 *al.*, 2017]. Although model complexity by itself is not a guarantee of model performance, ED2
103 has had success in simulating inter-annual variation in carbon uptake [*Trugman et al.* 2016],
104 simulating forest growth for regions remote from the calibration sites [*Medvigy et al.*, 2009;
105 *Medvigy and Moorcroft*, 2012] and performed well within the North American Carbon Program
106 Site Synthesis [*Dietze and Moorcroft*, 2011; *Schwalm et al.*, 2010]. Despite these promising
107 results, it remains unclear what limits long term prediction for models such as ED2, that link land
108 surface dynamics with plant demography [*Fisher et al.*, 2018].

109 As a way to identify model limitations, ED2 has been coupled with a trait database (BETY,
110 betydb.org) and ecoinformatics software (PEcAn, pecanproject.org). This combination allows
111 for 1) a data-constrained estimate of parameter uncertainty and 2) a method to attribute the
112 contribution of each parameter to model output uncertainty [*LeBauer et al.*, 2013]. This
113 software also includes parameter random effects (Section 2.5.1), which is a way to recognize that
114 the trait data is composed of multiple distributions (i.e. collected from different sites, conditions)
115 thereby increasing the parameter uncertainty [*Dietze*, 2017a]. Overall, the workflow design of
116 PEcAn is amenable to an iterative approach where the attribution of parametric uncertainty
117 motivates targeted field research that is subsequently entered into the trait database [*Davidson*,
118 2012]. PEcAn and ED2 have been coupled previously to parameterize and simulate tundra
119 vegetation [*Davidson*, 2012], as well as biofuel crops, including switchgrass [*LeBauer et al.*,
120 2013] and hybrid poplar [*Wang et al.*, 2013]. PEcAn and ED2 were used previously in a cross-

121 biome uncertainty analysis of seventeen global PFTs [*Dietze, Serbin, et al., 2014*] which
122 identified growth respiration, water conductance, stomatal slope, plant mortality and quantum
123 efficiency as contributing the most uncertainty to NPP predictions at timescales from 1 to 10
124 years.

125 Whereas previous PEcAn-ED2 analyses have focused on short-term responses, this
126 manuscript evaluates the long term (100 year) carbon sequestration in an unmanaged ecosystem
127 to help improve the prediction of long term forest and carbon dynamics. Specifically we ask
128 three key questions: 1) what ecological processes are most important for projecting long term
129 carbon uptake?, 2) can the ecological processes that contribute most to long term carbon uptake
130 uncertainty be improved through observational system studies or from further mechanistic
131 (model) development? and 3) do the most important processes change as a function of time?
132 Furthermore, we address these questions while considering parameter heterogeneity (i.e.
133 parameter random effects), which to our knowledge has not been addressed before for any
134 ecosystem model.

135 We perform this analysis at the Willow Creek eddy covariance site in Northern Wisconsin
136 [*Cook et al., 2004*], part of the Ameriflux network of sites within the Chequamegon Ecosystem-
137 Atmosphere Study. This site is ideal because it has a long-term flux record with considerable
138 ancillary biological data, and is representative of the larger region having experienced both
139 climate change [*Woods, 2000*] and disturbance [*Desai et al., 2005*]. In this way we anticipate
140 our findings will be applicable to a broader area across North America with similar ecosystem
141 type. To address the key questions we vary the model parameters within ED2 to estimate what
142 ecological processes contribute the most to model uncertainty according to model output (NEE,
143 NPP, AGB) and simulation time (1, 10, 100 years).

144

145 **2 Methods**

146 The methods section describes the way ED2 simulates ecosystems (Section 2.1) focusing
147 particularly upon the most influential ED2 parameters (Section 2.2). Next, we define the model
148 boundary conditions, including forest composition (Section 2.3) and atmospheric conditions
149 (Section 2.4). Section 2.5 describes the parameter calibration procedure intended to match
150 simulated and observed behavior at the Willow Creek site. Finally, we describe how PEcAn is
151 used to target areas in the model that contribute most to uncertainty (Section 2.6).

152 **2.1 Ecosystem Demography Model (Version 2)**

153 The Ecosystem Demography model, version 2 (ED2) is a land surface model capable of
154 simulating fluxes of carbon, nitrogen, sensible and latent heat between the atmosphere, forest
155 canopy, and soil. It accomplishes this through representation of important biological and
156 physical processes including photosynthesis [Farquhar *et al.*, 1980], soil carbon cycling [Bolker
157 *et al.*, 1998; Parton *et al.*, 1988], soil hydrology [Walko *et al.*, 2000], and leaf phenology [Botta
158 *et al.*, 2000]. Although ED2 explicitly tracks nitrogen, nutrient limitation is turned off for these
159 simulations to reduce the complexity of the processes controlling carbon exchange and limit the
160 parameters contributing to model uncertainty. ED2 tracks stand- and landscape-processes by
161 modeling the dynamics of cohorts (i.e. trees of identical plant function type, biomass and stem
162 density) and patches (i.e. groups of cohorts with similar stand age). The evolution of each cohort
163 (i.e. changes in stem density from mortality and disturbance, biomass from growth) is governed
164 by the biological and physical processes represented in the model conditioned upon the size and
165 age since last disturbance. Additional specifics of the model structure and operation have been
166 described in detail elsewhere [Medvigy *et al.*, 2009; Medvigy, 2006; Moorcroft *et al.*, 2001].
167 Here, we focused on a mechanistic description tailored specifically to the parameters that were
168 varied during the sensitivity analysis (section 2.2). These parameters were chosen because they
169 1) represented ecological processes that were important for previous sensitivity analyses with
170 ED2 simulations [Dietze, Serbin, *et al.*, 2014; LeBauer *et al.*, 2013; Medvigy *et al.*, 2009; Wang
171 *et al.*, 2013] and 2) were influential in preliminary long term carbon sequestration simulations
172 performed for this study.

173 **2.2 ED2 Parameter Description**

174 The complete list of parameters varied in our sensitivity analysis (Table 1) were chosen
175 based on the criteria listed at the end of Section 2.1. A parameter description is provided here
176 (parameters listed *in italics*) with more details located in the supporting information (Text S1) or
177 Rogers *et al.*, [2017]. Gross primary productivity (GPP) is represented by a standard enzyme-
178 kinetic model, which describes a plant's demand for carbon as the minimum between the light
179 limited (influenced by *quantum efficiency*) and enzyme limited reaction rate (influenced by
180 *V_{cmax}*) during photosynthesis [Farquhar *et al.*, 1980]. The *quantum efficiency* is the maximum
181 molar efficiency at which absorbed photosynthetically active radiation is converted into
182 assimilated CO₂, whereas *V_{cmax}* controls the maximum rate of CO₂ assimilation performed by

183 the Rubisco enzyme. Photosynthetic and transpiration rates are coupled through the leaf stomatal
184 conductance (influenced by *stomatal slope*) following the *Leuning*, [1995] variant of the Ball-
185 Berry model [*Ball et al.*, 1987]. Photosynthesis and transpiration are further reduced by water
186 stress which is calculated as the product of a *water conductance* parameter, available ground
187 water and fine root biomass. The water conductance parameter is an empirical attempt to
188 estimate the resistance of water flow from the soil to leaf. If the water supply does not meet the
189 canopy water demand, calculated based on the stomatal conductance and vapor pressure deficit,
190 the GPP and transpiration are scaled down. The *specific leaf area (SLA)* is the leaf surface area
191 per unit mass of leaf carbon and determines the amount of leaf surface area available to absorb
192 light for photosynthesis and for transpiration. Plant (autotrophic) respiration is the sum of leaf
193 maintenance respiration, root maintenance respiration and growth respiration (all plant tissues).
194 The leaf and root respiration is modeled as a function of respiration rate parameters (*leaf*
195 *maintenance rate*, *root respiration rate*), biomass and temperature. The growth respiration is
196 modeled as a fixed fraction (*growth respiration parameter*) of the previous days carbon balance.
197 The *root turnover* parameter is a coefficient that determines the (turnover) rate at which fine
198 roots are transferred to the litter pool. The *root to leaf allocation ratio (root2leaf)* parameter
199 determines how the active biomass carbon pool (B_a) is partitioned between roots and leaves, and
200 assumes that these pools are always in a fixed ratio. If the active biomass carbon pool exceeds
201 exceeds the allometric expectation based on cohort tree diameter the excess carbon is assigned to
202 a storage pool (B_{storage}). The *reproductive allocation (r_fract)* parameter is the fraction of B_{storage}
203 that is allocated to reproduction (seed). The *minimum height of reproduction* parameter defines
204 the minimum height of a tree before it can devote carbon to seed. Carbon-balance tree mortality
205 is calculated as an exponentially decreasing function with a decay rate parameter (*mort2*). The
206 likelihood of carbon-balance mortality decreases as the cumulative carbon balance (sum of GPP,
207 plant respiration and litter fluxes) for a cohort approaches the maximum possible cumulative
208 carbon balance (i.e. cohort at top of canopy). This is meant to account for shading competition
209 between cohorts. The density independent mortality parameter, *mort3*, is the background
210 mortality rate in the absence of competition taking into account processes like wind and insect
211 damage.

212 **2.3 Prescription of Initial Vegetation Conditions**

213 Willow Creek is located within the Chequamegon National Forest in northern Wisconsin.
214 The site is a secondary deciduous broadleaf forest recovering from a 1930 clearcut harvest and
215 consists primarily of sugar maple, red oak, birch, and basswood tree species. Flux tower
216 observations [Cook *et al.*, 2004] have recorded carbon, sensible and latent heat fluxes since 1998.
217 Both witness tree data [Liu *et al.*, 2011] and a land cover data set developed by the Wisconsin
218 Initiative for Statewide Cooperation on Landscape Analysis and Data (WISCLAND; Figure 1)
219 are used to define the forest species composition (Figure S1), tree diameter and stem density at
220 the start of the model simulation during the year 1900. See the supporting information (Text S2)
221 for more details. The soil carbon pools were initialized from contemporary observations of soil
222 carbon located at the nearby Sylvania Forest in northern Wisconsin [Tang *et al.*, 2009]. It was
223 assumed that the observed soil carbon at Sylvania Forest is comparable to Willow Creek (ca.
224 1900) as both sites would, in 1900, have been old growth forests (>300 years since last
225 disturbance).

226

227 **2.4 Prescription of Atmospheric Conditions**

228 The meteorology forcing data used here combined the multi-decadal trends of CRU-NCEP
229 (Climate Research Unit, National Centers for Environmental Prediction) meteorology product
230 (1901-2010), with the site level, high temporal resolution observations from the Willow Creek
231 flux tower (1998-2006) [Ricciuto *et al.*, 2013]. We provided meteorological forcing to ED2 at 30
232 minute resolution for air temperature, precipitation rate, wind speed, specific humidity, air
233 pressure, longwave radiation and shortwave radiation. The details of this method are provided in
234 the supporting information (Text S3, Figure S2). ED2 requires specific frequency bands of
235 radiation to run, therefore we used an algorithm [Weiss and Norman, 1985] to partition the total
236 shortwave radiation into direct (visible and infrared) and diffuse (visible and infrared)
237 components based upon the potential shortwave radiation from a cloudless sky as function of
238 time of year, time of day, and location.

239 The monthly atmospheric CO₂ concentration time series at Willow Creek was derived
240 from the annual mean atmospheric CO₂ from both the Law Dome record [Etheridge *et al.*, 1998]
241 and Mauna Loa Observatory record [Thoning *et al.*, 1989]. The average seasonal cycle of

242 atmospheric CO₂ as measured from the 1998-2006 flux tower records at Willow Creek was
243 added to the Law Dome/Mauna Loa record to estimate Willow Creek atmospheric CO₂ from
244 1901-2010 (Figure S2).

245 **2.5 Prescription of Parameter Values**

246 The Predictive Ecosystem Analyzer (PEcAn) ecoinformatics software version 0.3.2
247 (www.pecanproject.org) was used to assign parameter values (Section 2.2) within the ED2
248 model. This occurred in two main steps: 1) the parameter prior distributions and trait data were
249 queried from the BETY Database (www.betydb.org), and 2) the trait and parameter priors were
250 combined to estimate posterior parameter distributions within a hierarchical Bayesian meta-
251 analysis. These posterior parameter distributions (with some modifications, see Section 2.5.2)
252 were later used within ED2 to perform the simulations at Willow Creek. To help simplify this
253 analysis only posterior parameter values for the late hardwood PFT were calculated. The
254 parameters were fixed to the median value of the prior distribution for the early and mid
255 hardwood PFTs, as well as for late hardwood PFT parameters where trait data was not available.

256 **2.5.1 Defining Parameter Distributions: Bayesian Meta-analysis**

257 The BETY database (<https://www.betydb.org>) contains a library of prior parameter
258 distribution information and trait data culled from published and unpublished studies. In practice,
259 trait data were not available for every parameter; therefore parameters without trait data used the
260 prior distributions for model simulations. The trait data in this study (e.g. Table S1; last access
261 January 2014) were based upon field data or summary statistics collected from literature where
262 the subscripts represented a specific site (*i*) and treatment (*j*) combination. The meta-analysis
263 combines trait data from multiple studies and incorporates prior knowledge in a Bayesian
264 approach to estimate the posterior probability of each parameter. PEcAn uses the trait data and
265 priors to inform a linear mixed model for the unobserved ‘true’ trait mean Θ_{ij} ,

$$266 \quad \Theta_{ij} = \beta_0 + \beta_{site(i)} + \beta_{tr|site(ij)} + \beta_{gh} I(i), \quad (1)$$

267 which is a combination of the global trait mean (β_0), a Normal random effect for study site (
268 $\beta_{site(i)}$) (i.e. accounts for spatial influence of topography, soil etc.) , a nested Normal random
269 effect for any experimental treatments ($\beta_{tr|site(ij)}$) (i.e. accounts for influence of temperature,
270 nitrogen etc.), and a fixed effect for greenhouse studies (β_{gh}) [*LeBauer et al.*, 2013]. The term

271 $I(i)$ is an indicator variable set to 0 for field studies and 1 for studies conducted in a greenhouse,
272 growth chamber, or pot experiment. The posterior median for β_0 , is the nominal parameter
273 value input to ED2, and subsequently varied according to the posterior distribution of β_0 to
274 perform the sensitivity and ensemble analysis. PEcAn uses JAGS software version 2.2.0
275 [Plummer, 2010] to fit the meta-analysis model. More details on the linear mixed model and the
276 fitting procedure can be found in [LeBauer et al., 2013] and the supporting information (Text
277 S4). The random effects of site and treatment can be switched off within the meta-analysis,
278 which assumes all the trait observations are taken from the same population. We calculated the
279 posterior distributions both with (default) and without random effects in this analysis. During
280 the solution of the meta-analysis model all parameter MCMC chains (4 per parameter) are tested
281 for convergence according to the Gelman-Brooks-Rubin convergence criteria [Gelman and
282 Rubin, 1992].

283 2.5.2 Implementing the Posterior Parameters at Willow Creek

284 All simulations were run from June 1901 to January 2010, with initial vegetation
285 conditions defined by the witness tree data (Section 2.3) and atmospheric conditions (Section
286 2.4). A clearcut harvest was imposed within the model during the spring of 1930 by removing
287 all aboveground biomass, and 99% of the below-ground biomass. The removal of the below-
288 ground biomass was necessary to avoid unrealistic and vigorous re-sprouting of the forest
289 immediately after the clearcut. All of the harvested biomass was removed from the site and did
290 not contribute to soil carbon or carbon emissions.

291 A preliminary simulation was run with posterior median parameter values estimated using
292 the Bayesian meta-analysis within PEcAn (see Section 2.5.1) to test whether these parameters
293 provided reasonable growth dynamics and present day conditions. The criteria for reasonable
294 growth dynamics were 1) early and mid hardwood PFTs were succeeded by the late hardwood
295 PFT, consistent with the current state of the forest stand and 2) the final simulated forest stand
296 state variables of AGB, average NEE, and LAI distribution roughly matched the contemporary
297 observations. If these criteria were not met, parameter values were adjusted accordingly. This
298 preliminary simulation led to the growth of the early and mid hardwood dominating the late
299 hardwood PFT which disagreed with present day observations (Table S2). We improved the
300 simulated behavior by increasing the carbon balance morality parameter ($mort2$) from 20 yr^{-1} to
301 3.5 yr^{-1} and 7.0 yr^{-1} for the early and mid hardwood PFTs respectively. Next, the carbon balance

302 of the late hardwood PFT was increased by raising the quantum efficiency from 0.045 umol CO_2
303 $(\text{umol photon})^{-1}$ to 0.06 $\text{umol CO}_2 (\text{umol photon})^{-1}$ for the late hardwood PFT, which is
304 consistent with previous quantum efficiency syntheses [Singsaas *et al.*, 2001]. After these
305 parameter adjustments the successional behavior was more reasonable with the late hardwood
306 PFT catching up (LAI) or surpassing (AGB) the other PFTs by the year 2010 (Figure 2). This
307 adjusted parameter simulation was considered sufficient as a starting point given that the
308 simulated AGB and LAI were within 18 % and 5 % of observations respectively (Table S2).
309 While the simulated average NEE at Willow Creek from 2000-2005 ($-88 \text{ gC/m}^2/\text{yr}$) was a
310 smaller net sink than the site observations ($-223 \text{ gC/m}^2/\text{yr}$) (Table S2), the simulated NEE value
311 falls within the flux measurements within the Chequamegon National Forest Region region
312 including WLEF [Davis *et al.*, 2003] and Sylvania [Desai *et al.*, 2005]. In addition, the goal was
313 to provide a reasonable starting point for the uncertainty analysis, and not to obtain the best
314 overall fit to the observations. The complete list of posterior median parameter values (with
315 *mort2* and quantum *efficiency* hand adjustments) used in the ED2 simulations are shown in Table
316 1.

317

318 **2.6 Model Predictive Uncertainty and Model Parameter Sensitivity**

319 PEcAn estimates both the model predictive uncertainty and model parameter sensitivity
320 based upon both the prior and posterior parameter distributions from the meta-analysis with hand
321 adjustments (Section 2.5.2). The ensemble analysis estimates the distribution of the ED2 model
322 output from an ensemble of model runs based upon the sampling of the parameter distribution
323 using standard Monte Carlo techniques. The ensemble sampling assumes that there is no
324 correlation between parameters. This allows for the uncertainty in model outputs to be estimated
325 (e.g. mean, standard error, credible interval) providing the uncertainty in the model input
326 parameters. To estimate model sensitivity to each parameter, the model was evaluated at
327 $\pm(1,2,3) \sigma$ quantiles of the parameter being analyzed with all other parameters held at their
328 median values. The uncertainty analysis estimates the contribution of each parameter to the total
329 uncertainty in the model output. The contribution of a parameter to the uncertainty in model
330 output depends upon the uncertainty in the parameter and the sensitivity of model output to
331 changes in that parameter. The parameter uncertainty is transformed into the model uncertainty
332 by fitting a cubic polynomial function (spline), g_p , to the model output from the sensitivity

333 analysis. The partial variance, or fraction of the total variance contributed by parameter p , is
334 then estimated as,

$$335 \quad \text{partial variance}_p = \frac{\text{Var}[g_p(\beta_{op})]}{\sum_{p=1}^m \text{Var}[g_p(\beta_{op})]}, \quad (2)$$

336 where ‘Var’ represents the variance operator, m is the total number of parameters that are
337 varied, g is the fitted spline function, and β_o is the Monte Carlo sample of posterior parameter
338 values at which the spline is evaluated. To aid in the interpretation of partial variance, PEcAn
339 reports two dimensionless metrics summarizing the two components of the calculation
340 (parameter uncertainty and model sensitivity). The first metric is the parameter coefficient of
341 variation which is the posterior standard deviation divided by the posterior mean. The second
342 metric is the elasticity, which is the sensitivity (derivative of g_p) at the median parameter value
343 multiplied by the parameter median over the model output median. This partial variance
344 calculation is a univariate approach and does not account for the interaction between parameters.
345 Nevertheless, the extent to which parameter interactions influence the model variance can be
346 estimated by considering the ensemble variance. Following *LeBauer et al.* (2013) the ensemble
347 variance and the univariate estimate of variance are related by

$$348 \quad \text{Var}[f(\boldsymbol{\beta}_o)] = \sum_{p=1}^m \text{Var}[g_p(\beta_{op})] + \omega. \quad (3)$$

349 Equation (3) states that the full ensemble variance is equal to the univariate variance and
350 a parameter interaction term ω . The computational expense of the ED2 model limits the number
351 of ensemble members. The minimum number of members required to quantify the total variance
352 was estimated by evaluating the ensemble variance as a function of the number of ensemble
353 members. It was assumed an acceptable number of ensemble members is reached when the
354 ensemble variance reaches a constant value.

355

356 2.6.1 Implementing the Uncertainty Analysis at Willow Creek

357 The contribution of model parameter uncertainty to the model predictive uncertainty was
358 evaluated by performing an uncertainty analysis for model outputs net ecosystem exchange
359 (NEE), net primary productivity (NPP), and above-ground biomass (AGB). The parameter
360 contribution to model uncertainty was evaluated for early (1935-1940), mid (1935-70), and late

361 (1935-2009) time frames of the model output. For simplicity these are referred to as annual,
362 decadal, and centennial time frames respectively hereafter. These time frames were chosen to
363 capture the growth and succession behavior after the imposed clearcut of 1930.

364 For this analysis all conifer, early, and mid hardwood PFT parameters were fixed to their
365 median values, and only the 15 late hardwood PFT parameters were allowed to vary across their
366 parameter distributions. This was done to reduce the computational expense because each PFT
367 has a separate parameter set. In addition it is hypothesized that the overall forest stand dynamics
368 at Willow Creek is most sensitive to the late successional PFT given that this PFT dominates the
369 present day forest.

370 This analysis was repeated for three separate parameter distributions: 1) prior only, 2)
371 posterior (where trait data were available) and 3) posterior (where trait data were available) with
372 random effects. The prior distributions used no trait data, only including the prior knowledge of
373 the parameter distribution [Dietze, Serbin, et al., 2014]. The posterior distribution assimilates
374 trait data through the meta-analysis approach (Section 2.5.1) but assumes no across-site and
375 across-treatment variability (Equation 1). The posterior with random effects, hereafter referred
376 to as ‘posterior_re’, also assimilates trait data but accounts for across-site and across-treatment
377 variability. Unless otherwise noted, the posterior_re is the default posterior within the results
378 and discussion, and we discuss how this methodology influenced the results (Section 4.3).

379 For clarity and consistency when discussing elements of the sensitivity analysis, the
380 uncertainty in the parameter values are referred to as *parameter uncertainty (estimated by CV)*,
381 the inherent model response to changes in a parameter is referred to as *sensitivity (estimated by*
382 *elasticity)*, and the variation in model output is referred to as *model uncertainty (estimated by*
383 *partial variance)*.

384 2.6.2 Parameter Interactions

385 We used parameter interactions to identify the remaining parameters that significantly
386 contributed to model uncertainty and were not identified within the one-at-a-time sensitivity
387 analysis (Section 2.6). These interactions were quantified by identifying correlations between
388 pairs of parameters within a filtered ensemble analysis. First, for every parameter combination a
389 scatter plot was populated from the normalized parameter values defined by the ensemble.
390 Second, parameter combinations were removed [e.g. Knutti et al., 2002; Sriver et al., 2012] that

391 led to model output outside the bounds of the NEE and AGB observations. Third, parameters
392 were considered to interact if the filtered parameter pairs were significantly correlated.

393 The observations used to filter the parameter values were the average NEE from 2000-2005
394 as calculated by aggregated flux tower data [Ricciuto *et al.*, 2013] and contemporary remotely
395 sensed biomass data [Kellndorfer *et al.*, 2012]. Remotely sensed biomass data were chosen
396 instead of plot level, allometric based biomass estimates because it was more consistent with the
397 spatial region from the witness tree data and likely provides a more realistic estimate of biomass
398 variability. The observed mean biomass at Willow Creek was estimated from the average
399 biomass of the 3x3 km² region composed of 30x30 m² grid cells surrounding the Willow Creek
400 forest stand. The acceptable range in the average biomass was estimated by the variation in the
401 1x1 km² subgrid regions. Following Barr *et al.*, [2009] the uncertainty of the NEE was
402 estimated by accounting for uncertainty from 1) limited sampling of turbulent eddies, 2) the
403 choice of friction velocity filtering threshold, and 3) the gap-filling algorithm for missing flux
404 data.

405 **3 Results**

406 **3.1 Prior and posterior parameters distributions**

407 The late hardwood PFT parameter distribution for the prior, posterior, and posterior_re are
408 described in Table 2 and Figure 3. Trait data were available for the meta-analysis for 5 out of the
409 15 parameters: fine root/leaf allocation, SLA, leaf respiration rate, V_{cmax} , and *quantum efficiency*.
410 The reduction in parameter spread (CI range) between the prior and posterior_re was 70%, 77%,
411 82%, 62% and 47% respectively, whereas the prior to posterior reduction in spread was much
412 greater (97%, 99%, 99%, 97%, 98%).

413 **3.2 Ensemble Spread for simulated NEE, NPP and AGB**

414 The ensemble spread of all model output was strongly dependent upon the parameter
415 distribution (Figure 4) where the CI range decreased in order from prior to posterior_re to
416 posterior. The 95% confidence interval of the ensemble prior ranged from 101-1471 gC m⁻² yr⁻¹
417 for NEE, 616-2834 gC m⁻² yr⁻¹ for NPP, and 4-48 kgC m⁻² for AGB. The CI ranges reduced by
418 48%, 42% and 70% from the prior to the posterior_re ensemble, and by 80%, 72% and 76% from
419 the prior to posterior ensemble for NEE, NPP and AGB respectively.

420 3.3 Sensitivity and uncertainty analysis: 1935-2009 time frame

421 The model uncertainty based upon the posterior_re parameter distribution was dominated
422 by the influence of the *quantum efficiency*, *leaf respiration rate*, and *water conductance* (Figure
423 5). *Quantum efficiency* and *leaf respiration rate* dominated uncertainty due to a combination of
424 a moderate coefficient of variation (i.e. prior parameter distribution is relatively diffuse) and high
425 absolute elasticity (i.e. the model NEE was highly sensitive to parameter changes). Although
426 *water conductance* was much less constrained relative to *quantum efficiency* and *leaf respiration*
427 *rate*, the partial variance was lower as a result of the lower elasticity. Overall this led to model
428 uncertainty contributions of 40%, 18% and 13% for *quantum efficiency*, *leaf respiration rate* and
429 *water conductance* respectively (Figure 6).

430 When considering the posteriors without random effects, on the other hand, *quantum*
431 *efficiency* and *leaf respiration* were more constrained (96% and 97% reduction in CI
432 respectively) which reduced the simulated contemporary ensemble spread by 72% and 60% for
433 NEE and AGB respectively (Figure 4). As a result of this increased constraint, NEE was most
434 influenced by *water conductance* (37%), *reproductive allocation* (24%), *growth respiration*
435 (20%), *mort2* (9%), *stomatal slope* (3%), and *minimum height* for reproduction (4%) (Figure 7).

436 3.4 Parameter importance by model output (NEE, NPP, AGB) and time (annual, 437 decadal, centennial)

438 The results of the uncertainty analysis based on the posterior_re distribution were similar
439 regardless of model output (NEE, NPP, AGB) and time frame (annual, decadal, centennial)
440 (Figure 7). In all cases the model was most sensitive to *quantum efficiency*, followed by *leaf*
441 *respiration rate* and *water conductance* parameters. The uncertainty analysis based upon the
442 posterior distribution (without random effects), on the other hand, was moderately dependent
443 upon the type of model output, but mostly robust to time frame (Figure 7). The average NEE
444 and average AGB were influenced by a wide range of parameters including *water conductance*,
445 *reproductive allocation*, *growth respiration*, and *mort2*, accounting for approximately 90% of the
446 total variation. In contrast, the average NPP was affected primarily by only *growth respiration*
447 and *water conductance* accounting for approximately 90% of the total variation. These results
448 remained relatively unchanged whether the annual partial variance was taken early in the

449 simulation (i.e. years 1935-1940) as shown in the figures or late in the simulations (i.e. years
450 2000-2005).

451 **3.5 Parameter interactions**

452 The uncertainty analysis did not directly account for parameter interactions because it was
453 based upon varying one parameter at a time while all other parameters were fixed at their median
454 values. In an attempt to quantify the impact of parameter interactions upon model behavior, the
455 ensemble variance was compared to the univariate uncertainty analysis estimated variance (Table
456 S3). The multivariate ensemble reduced the simulated standard deviation by more than 50% for
457 all model outputs implying significant parameter interactions (Table S3). This finding held true
458 across all time frames (not shown).

459 Second order (pairwise) parameter interactions (posterior_re only) were identified by
460 considering those parameter pairs from ensemble members that fell within the observed range for
461 NEE (Figure S3), and both AGB and NEE (Figure S4). Out of 105 possible parameter pairs
462 only 8% were correlated with a 95% certainty when filtering simulated NEE to match the
463 observed range, whereas the combined NEE and AGB filter identified 4% of the parameter pairs
464 as correlated. Considering the most important parameters in determining model uncertainty from
465 the univariate analysis (*quantum efficiency*, *leaf respiration*, *water conductance*, and *growth*
466 *respiration*), only 3 parameters (*root turnover rate*, *root2leaf*, V_{cmax}) correlate when using NEE
467 as a filter (Figure S3). When NEE and AGB are used as a filter there are only 2 instances of
468 correlation: *quantum efficiency* versus *stomatal slope* and *growth respiration* versus *minimum*
469 *height* (Figure S4).

470 **4 Discussion**

471 **4.1 Highest Contributions to Carbon Uptake Uncertainty**

472 The parameters of *quantum efficiency* and *leaf respiration rate* were the highest
473 contributors to model uncertainty (Figure 6) regardless of time frame (annual, decadal,
474 centennial) and predictive variable (e.g. NEE, NPP, AGB). The contribution to model
475 uncertainty was primarily from parametric uncertainty, despite a significant reduction in the 95%
476 CI range from the prior distribution (47 and 86% for quantum efficiency and leaf respiration
477 respectively). Although each parameter was subject to constraint by 13 and 44 sources of trait

478 data respectively (Table 2), the effective sample size for reducing the posterior uncertainty was
479 much lower (4 and 7 total sites respectively). Therefore the parameter uncertainty within the
480 random effects model (i.e. within-site, across site, treatment, greenhouse parameters) remain
481 poorly constrained (Table S4). *Leaf respiration rate* is a fundamental physiological process tied
482 to leaf cellular maintenance, while the *quantum efficiency* describes the initial slope of the
483 relationship of photosynthesis to light and regulates the rate of carbon uptake under sub-
484 saturating conditions, and varies substantially across TBMs [Rogers *et al.* 2017]. Given that
485 these parameters represent different controls on CO₂ fluxes and are fundamental to the
486 understanding of ecosystem processes, are included in almost all TBMs [Rogers *et al.* 2017], and
487 can be measured simultaneously using direct, leaf level photosynthetic light response curves,
488 more field observations of these traits should be made a priority.

489 The *water conductance* parameter contributed the next most to model uncertainty in part
490 because there was no trait data to provide constraint (i.e. not a directly observable trait).
491 Assimilation of tower-based latent heat fluxes have the potential to inform the water conductance
492 parameter, however this is a weak constraint because tower-based latent heat fluxes do not
493 distinguish between evaporation and canopy transpiration [Medvigy *et al.*, 2009]. Sap flux is a
494 direct measure of stem transpiration and would likely provide a better constraint [Dietze, Serbin
495 *et al.*, 2014], however, given the formulation in ED2, this approach also requires well-
496 constrained estimates of LAI, stomatal slope, soil moisture, and fine root biomass. A better
497 approach to representing water stress is to implement a hydraulic conductance model [Sperry
498 *and Love*, 2015] thereby eliminating the need for an overall water conductance parameter.
499 Hydraulic conductance models explicitly simulate water supply to the leaf through plant trait
500 measurements (e.g. conductance across plant tissues, and water potential at reduced
501 conductivity). Such a model has been included in a recent update to ED2 [Xu *et al.*, 2016] and
502 could be constrained with existing databases for hydraulic traits [Bartlett *et al.*, 2016; Choat *et*
503 *al.*, 2012]

504 The reproductive allocation parameter contributed highly to model output uncertainty, in
505 contrast with previous ED2 uncertainty analyses [LeBauer *et al.*, 2013; Wang *et al.*, 2013;
506 Dietze, Serbin, *et al.*, 2014]. This is not surprising given the relatively short simulation length
507 (<10 years) for these studies. This finding demonstrates that the cumulative impact of the carbon
508 allocated to reproduction versus structural growth (see Section 2.2) is important for long-term

509 carbon dynamics. Observations and improved mechanistic description related to recruitment rate
510 could offer reduced model uncertainty [e.g. *Schupp and Jordano, 2011*]. Within ED2, the
511 observed recruitment rate is a function of both the allocation of carbon to reproduction and a
512 composite loss rate that combines seed and seedling mortality along with non-seed reproductive
513 allocation (e.g. flowers, nectar, pollen), which are highly conceptualized (non-mechanistic)
514 parameters. For this analysis the loss rate was fixed at 95% because the correlation (equifinality)
515 between these two parameters makes it challenging to constrain each individually. In a more
516 recent implementation of ED2, the seedling mortality of aspen and black spruce are constrained
517 by growth trends and germination experiments with mortality increasing with organic layer depth
518 [*Trugman et al., 2016*]. In general, a more detailed model representation of the processes that
519 control the carbon allocated to reproduction, seed dispersal and sapling survival is needed and an
520 active topic of research [e.g. *Clark et al., 2012*]. A particularly important question is to what
521 degree large scale models need to represent distance- and density-dependent mechanisms of
522 mortality that go beyond carbon balance, such as seed and seedling predation and disease, which
523 have long been thought to play a large role in population stability and the maintenance of
524 biodiversity [*Bagchi et al., 2014; Dietze and Matthes, 2014; Janzen, 1970*].

525 Growth respiration contributed significantly to carbon uptake uncertainty consistent with
526 earlier ED2 studies at shorter time scales across multiple biomes [*Dietze, Serbin et al., 2014*],
527 poplar [*Wang et al., 2013*] and switchgrass [*LeBauer et al., 2013*] sites. Given the multitude of
528 plant tissue building processes the growth respiration factor is intended to represent [*Medvigy et*
529 *al., 2009*], it is challenging to observe directly. A more detailed approach to represent growth
530 respiration is through a pathway analysis approach [*Penning de Vries et al., 1974*]. This method
531 accounts for the fact that biosynthesis costs are dependent upon the type of biochemical
532 compounds (i.e. protein, carbohydrates, lipids, lignin and organic acids) and their abundance in
533 different plant tissues (e.g. leaf, stem, root). This approach is being implemented in PEcAn,
534 however, a significant bottleneck is that plant trait databases need more plant tissue composition
535 data to make use of the additional mechanistic complexity.

536 The carbon balance mortality parameter (*mort2*) only fell within the top half of all
537 parameters contributing to uncertainty. This outcome was unexpected given the length of the
538 simulation and the fact that long-lived trees are known to be highly sensitive to mortality rate
539 [*Caswell, 2001; Franco and Silvertown, 1996*]. This may have occurred for several reasons.

540 First, this analysis was based upon the uncertainty of the site-level model output (i.e. not PFT
541 specific) while varying the parameters for the late hardwood PFT only. It is possible that
542 imposing a high mortality rate upon the late hardwood PFT did not significantly impact the
543 development of the overall forest stand carbon dynamics and biomass because of compensating
544 effects from the early and mid hardwood PFTs (see Section 4.4). Second, the version of ED2
545 used in this analysis calculates the carbon balance mortality as a function of carbon balance
546 based on light competition, ignoring any contribution to mortality from hydraulic limitation
547 (drought mortality). Finding observations to inform the carbon balance mortality rate is
548 challenging given the long life span of trees [Dietze and Moorcroft, 2011] and the difficulties in
549 directly measuring the carbon balance of trees in the field [Dietze, Sala, et al., 2014; Mantoosh,
550 2017].

551 We found no compelling evidence that parameter interactions significantly altered the
552 evaluation of important parameters in this analysis. The 50% reduction between the ensemble
553 variance and sum of the univariate variance (Table S3), demonstrates significant parameter
554 interaction, however, this was not surprising given that ED2 is a mechanistically detailed and
555 non-linear model. The bivariate approach (Section 2.6.2) identified overall weak parameter
556 correlations given 8% and 4% of all possible parameter combinations were correlated to 95%
557 certainty for NEE and NEE/AGB filtering, respectively. We expected 5% of the parameters to
558 have correlation purely by chance alone, suggesting interactions played a minimal role on the
559 results.

560 **4.2 Contributions to Model Uncertainty as a Function of Time**

561 The parametric contribution to uncertainty for modeled carbon uptake was generally the
562 same regardless of averaging time (Figure 7). This result was unexpected given that parameters
563 controlling carbon dynamics on short time scales (e.g. V_{cmax} , quantum efficiency, SLA, stomatal
564 conductance) were expected to dominate the uncertainty for sub-decadal time scales, whereas
565 parameters that control successional processes (e.g. mortality, reproductive allocation) were
566 expected to be more important at the centennial time scale. This result was consistent with the
567 finding of an across-site analysis using the ED2 model [Dietze, Serbin, et al., 2014], which was
568 based upon the response variable of NPP averaged for a relatively short time (<10 years). The
569 averaging time for the response variable was much greater for this analysis, and PFT succession
570 occurred (Figure 2). The parameter contribution to uncertainty may have remained constant

571 (across time) either because the largest predictive uncertainties were unrelated to successional
572 processes and/or were independent of the late hardwood PFT analyzed here. Furthermore,
573 important across-PFT parameter interactions that minimize the importance of parameters related
574 to succession could be missing.

575

576 **4.3 Impact of Random Effects upon Model Uncertainty**

577 Including random effects within the meta-analysis significantly broadened the posterior
578 distributions (e.g. leaf respiration and quantum efficiency; Figure 3) and subsequently changed
579 the relative parametric contributions to model uncertainty (Figure 7). If, however, we used the
580 same approach as previous ED2 analyses and exclude random effects, the findings were more
581 similar. For example, our estimate of parameter contribution to short-term model uncertainty
582 was similar for late hardwood [*Dietze, Serbin, et al., 2014*], early hardwood [*Wang et al., 2013*]
583 and grass [*LeBauer et al., 2013*], only when random effects were not considered (Tables 3, 4).
584 Specifically, the parameter contribution to uncertainty in NPP (<10 year average) found here was
585 similar for a late hardwood PFT (WLEF, Park Falls, Wisconsin; [*Dietze, Serbin, et al., 2014*])
586 (Table 3), with water conductance, growth respiration and stomatal slope contributing the most
587 uncertainty. Our uncertainty analysis based on short term AGB performed similarly to a poplar
588 (early hardwood) [*Wang et al., 2013*] with the highest contributors of growth respiration, leaf
589 respiration, quantum efficiency, mortality coefficient and water conductance (Table 4).

590 We chose to include random effects in this analysis for two reasons. First, the parameter
591 posteriors calculated without random effects led to a model spread that was unrealistically
592 narrow, likely underestimated the true predictive uncertainty, and was inconsistent with the
593 observations (Figure 4, panel B). Second, many ecological processes are heterogeneous,
594 therefore the assumption that spatially distributed trait data is drawn from the same distribution
595 (i.e. no random effects) may underestimate the true variability of the parameters fitted to the data
596 [*Dietze, 2017a*]. On the other hand, the practicality of implementing the random effects model,
597 which requires the estimation of additional model parameters (e.g. across-site precision, Table
598 S4) depends upon the availability of large amounts of trait data distributed across many study
599 sites. For example, 4 out of the 5 parameters that underwent meta-analysis had between 13-88
600 observations (sample mean for a particular species, site and treatment), however the number of

601 unique sites from which the trait data were measured was much less (range from 5-10 sites per
602 trait).

603 In general, parameter posterior distributions using random effects reflects contributions from
604 both the mean global trait *uncertainty* and across site and treatment *variability* (Section 2.6.1).
605 Whereas the parameter *uncertainty* can be reduced with observations, at least part of parameter
606 *variability* is irreducible and represents missing processes within the modeling system (process
607 error) [Dietze, 2017b]. In this study, the high variability arose, in part, because we grouped
608 plant species traits across time, location and species for the late successional PFT. In theory it
609 may be possible to reduce the parameter variability if this simulation was re-defined in terms of
610 species specific traits (e.g. maple, basswood, ironwood), however, in practice, observations were
611 lacking. Future work should pay close attention how an expanding trait database combined with
612 the precise classification of PFTs impact the posterior parameter distributions. Beyond
613 quantifying random effects through trait databases, the site-to-site variability captured by random
614 effects can also be estimated as part of Hierarchical Bayesian calibration approaches [Dietze,
615 2017a], which have recently been implemented in PEcAn [Fer et al., 2018]. Future studies
616 should estimate the parameter variability and quantify the impact upon predictive uncertainty
617 through this calibration approach.

618

619 **4.4 Experimental Design Improvements**

620 We have looked at the influence of a limited number of uncertainties upon model outcome to
621 serve as a preliminary test of the capabilities of PEcAn and the ED2 model. There are multiple
622 ways to improve the analysis in which to include a wider range of uncertainties [Dietze, 2017b].
623 This analysis focused upon parameters related to aboveground processes of plant succession and
624 growth, a strength of the ED2 model (Section 2.1). More attention should be paid in future
625 analyses to the model uncertainty related to soil initial conditions and below-ground carbon
626 cycling parameters, which had not yet been implemented in PEcAn at the time of this analysis.
627 The framework of the PEcAn software is amenable to adding initial conditions (e.g. soil carbon)
628 to the uncertainty analysis where the initial soil carbon is treated as an uncertain parameter. It is
629 probable that parameters related to soil biogeochemistry may provide a significant fraction of
630 prediction uncertainty provided that the initialization method of the soil carbon pool (i.e. the

631 empirical approach used in this analysis versus spinup) led to an 80% difference in century scale,
632 cumulative NEE (Figure S5). Although this difference in soil carbon is significant in absolute
633 terms the parameter sensitivity and contribution to model uncertainty for AGB and NPP (i.e.
634 growth processes) should not change appreciably because nitrogen limitation is turned off.
635 Furthermore, expanding this study to include uncertainties of above-ground initial conditions and
636 climate driver-data should provide a more comprehensive understanding of uncertainty beyond
637 the process/mechanistic uncertainty we focused on here.

638 Further analysis of model uncertainty should include direct quantification of second order
639 and total sensitivity indices. The number of parameters considered here (15) combined with the
640 computation time per centennial run (~10 hours) make variance based sensitivity approaches
641 inefficient. The elementary effects approach (i.e. method of Morris) [e.g. *Saltelli et al.*, 2008] is
642 appropriate for computationally intensive models with many factors (parameters). The method
643 provides an approach to prune or ‘fix’ parameters that are unimportant, and allows the parameter
644 space of important parameters to be explored more fully. This could make it feasible to expand
645 the uncertainty analysis to include parameters from the early, mid and late hardwood PFTS that
646 were fixed for this analysis.

647 Although we focused on the impact of the late successional PFT on model outcome, we
648 expect across-PFT parameter interactions to be important for forest growth. For example, a
649 parameterization unfavorable for a single PFT will likely promote the survival of another PFT as
650 they are in direct competition for resources. This compensating effect may explain why the
651 simulated NEE was relatively consistent regardless of the PFT composition. Across-PFT
652 interactions could be better isolated by 1) performing an across-PFT sensitivity analysis (e.g.
653 following elementary effects approach) upon a more limited set of parameters for each PFT or 2)
654 basing the sensitivity analysis on % composition variables of NEE, AGB or NPP instead of total
655 stand composition as was done here. A more recent version of PEcAn includes an estimate of
656 parameter correlations both within and across PFTs for seven leaf traits [*Shiklomanov*, 2018].
657 He found that including covariance within multivariate modeling reduced the mean trait
658 uncertainty, however, across-PFT correlations added little additional constraint. Given that
659 TBMs containing demographic representations are likely more sensitive to parameter
660 modifications that can impact competition and thus succession, but are becoming more favored
661 compared to big-leaf representations of canopies [*Fisher et al.*, 2018], it is essential to perform

662 analyses that can help to parameterize these models for long time scale simulations.
663 Furthermore, it is important to understand if the same processes that impose limitations to
664 predictive uncertainty at Willow Creek apply to other biomes.

665

666 **5 Conclusions**

667 This analysis finds that the leaf parameters of *quantum efficiency* and *leaf respiration rate*
668 contributed the most to long-term carbon exchange uncertainty. Other plant-scale parameters
669 that contributed significantly to model uncertainty include *water conductance*, *reproductive*
670 *allocation*, *growth respiration* and *carbon balance mortality*. Surprisingly, the relative
671 contribution of these parameters to model uncertainty remained mostly the same regardless of
672 model output or simulation time, but this could be because we focused on the carbon cycle while
673 other cycles could have yielded different results. These findings were dependent upon inclusion
674 of random effects (across-site and treatment variability) within the parameter optimization
675 methodology, which broadened the posterior parameter distributions. Excluding random effects
676 narrowed the posterior distributions and led to model projections that were inconsistent with
677 contemporary observations of NEE and AGB. In general, we recommend including random
678 effects within the PEcAn workflow, and rely on both an expanding database of trait observations
679 and hierarchical Bayesian calibration to reduce the parameter and model uncertainty.

680 It is hypothesized that additional reduction in model uncertainty can be achieved by a more
681 exhaustive search for trait-level data given that *quantum efficiency* and *leaf respiration* can be
682 measured simultaneously, however can be time consuming and laborious. We recommend
683 including more targeted integrative data constraints such as recruitment rate measurements for
684 *reproductive allocation*, and direct measure of non-structural carbohydrates to constrain *carbon*
685 *balance mortality*. Furthermore additional trait level data across multiple sites and multiple
686 samples should help constrain parameters that define the within and across site variation within
687 the meta-analysis thereby reducing the parameter CV. Parameters of growth respiration and
688 water conductance are also important but hard to constrain in demographic models, such as ED2
689 [Fisher *et al.*, 2018], therefore we recommend a re-structuring of the model formulation to allow
690 for direct measurements of the processes involved.

691

692
693
694
695
696
697
698
699
700
701
702
703
704
705
706
707
708
709
710
711
712
713
714
715
716

Acknowledgements

This work was supported by the National Institute for Climatic Change Research (NICCR) as part of the Terrestrial Ecosystem Science (TES) program managed by the U.S. Department of Energy’s Office of Biological and Environmental Research (BER). M. Dietze and PEcAn development were supported by NSF ABI #1062547 and #1458021 and NSF DIBBs #1261582, and S. Serbin was partially supported by NSF ABI #1062547 as well as the United States Department of Energy contract No. DE-SC0012704 to Brookhaven National Laboratory. We are grateful to David LeBauer for helpful discussions and support related to the functioning of ED2, PEcAn and BETY. We would also like to thank Ryan Knox for developing ED2 output visualization software and Doug Baldwin for providing assistance with remotely-sensed biomass data. Travel to the University of Illinois was funded by the National Science Foundation through an INTERFACE Student Exchange Travel Grant. Finally, thank you to IT services at Penn State and the University of Illinois. The data used within the manuscript are listed in the references, tables and supplements.

717 **References**

- 718 Arora, V. K., Boer, G. J., Friedlingstein, P., Eby, M., Jones, C. D., Christian, J. R., et al. (2013).
719 Carbon-Concentration and Carbon-Climate Feedbacks in CMIP5 Earth System Models.
720 *Journal of Climate*, 26(15), 5289–5314. <https://doi.org/10.1175/jcli-d-12-00494.1>
- 721 Bagchi, R., Gallery, R. E., Gripenberg, S., Gurr, S. J., Narayan, L., Addis, C. E., et al. (2014).
722 Pathogens and insect herbivores drive rainforest plant diversity and composition. *Nature*,
723 506(7486), 85–88. <https://doi.org/10.1038/nature12911>
- 724 Ball, J. T., Woodrow, I. E., & Berry, J. A. (1987). A Model Predicting Stomatal Conductance
725 and its Contribution to the Control of Photosynthesis under Different Environmental
726 Conditions. In J. Biggins (Ed.), *Progress in Photosynthesis Research* (pp. 221–224).
727 Springer Netherlands. https://doi.org/10.1007/978-94-017-0519-6_48
- 728 Barr, A. G., Hollinger, D., & Richardson, A. D. (2009). CO2 flux measurement uncertainty
729 estimates for NACP, *Eos Trans. AGU*, 90(52), Fall Meet. Suppl., Abstract B54A-04.
- 730 Bartlett, M. K., Klein, T., Jansen, S., Choat, B., & Sack, L. (2016). The correlations and
731 sequence of plant stomatal, hydraulic, and wilting responses to drought. *Proceedings of*
732 *the National Academy of Sciences*, 113(46), 13098–13103.
733 <https://doi.org/10.1073/pnas.1604088113>
- 734 Bolker, B. M., Pacala, S. W., & Parton, W. J. (1998). Linear Analysis of Soil Decomposition:
735 Insights from the Century Model. *Ecological Applications*, 8(2), 425–439.
736 [https://doi.org/10.1890/1051-0761\(1998\)008\[0425:LAOSDI\]2.0.CO;2](https://doi.org/10.1890/1051-0761(1998)008[0425:LAOSDI]2.0.CO;2)
- 737 Botta, A., Viovy, N., Ciais, P., Friedlingstein, P., & Monfray, P. (2000). A global prognostic
738 scheme of leaf onset using satellite data. *Global Change Biology*, 6(7), 709–725.
739 <https://doi.org/10.1046/j.1365-2486.2000.00362.x>
- 740 Braswell, B. H., Sacks, W. J., Linder, E., & Schimel, D. S. (2005). Estimating diurnal to annual
741 ecosystem parameters by synthesis of a carbon flux model with eddy covariance net
742 ecosystem exchange observations. *Global Change Biology*, 11(2), 335–355.
- 743 Caswell, H. (2001). *Matrix Population Models* (Second). Sunderland, Massachusetts: Sinauer
744 Associates.
- 745 Choat, B., Jansen, S., Brodribb, T. J., Cochard, H., Delzon, S., Bhaskar, R., et al. (2012). Global
746 convergence in the vulnerability of forests to drought. *Nature*, 491(7426), 752.
747 <https://doi.org/10.1038/nature11688>
- 748 Clark, J. S., Soltoff, B. D., Powell, A. S., & Read, Q. D. (2012). Evidence from Individual
749 Inference for High-Dimensional Coexistence: Long-Term Experiments on Recruitment
750 Response. *PLOS ONE*, 7(2), e30050. <https://doi.org/10.1371/journal.pone.0030050>
- 751 Cook, B. D., Davis, K. J., Wang, W. G., Desai, A., Berger, B. W., Teclaw, R. M., et al. (2004).
752 Carbon exchange and venting anomalies in an upland deciduous forest in northern
753 Wisconsin, USA. *Agricultural and Forest Meteorology*, 126(3–4), 271–295.

- 754 Davidson, C. D. (2012). The modeled effects of fire on carbon balance and vegetation abundance
755 in Alaskan tundra. M.S. Thesis, University of Illinois, Urbana-Champaign.
- 756 Davis, K. J., Bakwin, P. S., Yi, C., Berger, B. W., Zhao, C., Teclaw, R. M., & Isebrands, J. G.
757 (2003). The annual cycles of CO₂ and H₂O exchange over a northern mixed forest as
758 observed from a very tall tower. *Global Change Biology*, 9(9), 1278–1293.
759 <https://doi.org/10.1046/j.1365-2486.2003.00672.x>
- 760 Desai, A. R., Bolstad, P. V., Cook, B. D., Davis, K. J., & Carey, E. V. (2005). Comparing net
761 ecosystem exchange of carbon dioxide between an old-growth and mature forest in the
762 upper Midwest, USA. *Agricultural and Forest Meteorology*, 128(1–2), 33–55.
- 763 Dietze, M. C. (2017a). *Ecological Forecasting*. Princeton University Press.
- 764 Dietze, M. C. (2017b). Prediction in ecology: a first-principles framework. *Ecological
765 Applications*, 27(7), 2048–2060. <https://doi.org/10.1002/eap.1589>
- 766 Dietze, M. C., & Matthes, J. H. (2014). A general ecophysiological framework for modelling the
767 impact of pests and pathogens on forest ecosystems. *Ecology Letters*, 17(11), 1418–1426.
768 <https://doi.org/10.1111/ele.12345>
- 769 Dietze, M. C., & Moorcroft, P. R. (2011). Tree mortality in the eastern and central United States:
770 patterns and drivers. *Global Change Biology*, 17(11), 3312–3326.
771 <https://doi.org/10.1111/j.1365-2486.2011.02477.x>
- 772 Dietze, M. C., Lebauer, D. S., & Kooper, R. (2013). On improving the communication between
773 models and data. *Plant, Cell & Environment*, 36(9), 1575–1585.
774 <https://doi.org/10.1111/pce.12043>
- 775 Dietze, M. C., Serbin, S. P., Davidson, C., Desai, A. R., Feng, X., Kelly, R., et al. (2014). A
776 quantitative assessment of a terrestrial biosphere model's data needs across North
777 American biomes. *Journal of Geophysical Research: Biogeosciences*, 119(3),
778 2013JG002392. <https://doi.org/10.1002/2013JG002392>
- 779 Dietze, M. C., Sala, A., Carbone, M. S., Czimeczik, C. I., Mantooth, J. A., Richardson, A. D., &
780 Vargas, R. (2014). Nonstructural Carbon in Woody Plants. *Annual Review of Plant
781 Biology*, 65(1), 667–687. <https://doi.org/10.1146/annurev-arplant-050213-040054>
- 782 Etheridge, D. M., Steele, L. P., Langenfelds, R. L., Francey, R. J., Barnola, J. M., & Morgan, V.
783 I. (1998). Historical CO₂ records from the Law Dome DE08, DE08-2, and DSS ice cores.
784 In *Trends: A Compendium of Data on Global Change*. Carbon Dioxide Information
785 Analysis Center, Oak Ridge National Laboratory, U.S. Department of Energy, Oak
786 Ridge, Tenn., U.S.A.
- 787 Farquhar, G. D., von Caemmerer, S., & Berry, J. A. (1980). A Biochemical Model of
788 Photosynthetic CO₂ Assimilation in Leaves of C₃ Species. *Planta*, 149, 78–90.
- 789 Fer, I., Kelly, R., Moorcroft, P. R., Richardson, A. D., Cowdery, E. M., & Dietze, M. C. (2018).
790 Linking big models to big data: efficient ecosystem model calibration through Bayesian

- 791 model emulation. *Biogeosciences Discuss.*, 2018, 1–30. [https://doi.org/10.5194/bg-2018-](https://doi.org/10.5194/bg-2018-96)
792 96
- 793 Fisher, R. A., Koven, C. D., Anderegg, W. R. L., Christoffersen, B. O., Dietze, M. C., Farrior, C.
794 E., et al. (2018). Vegetation demographics in Earth System Models: A review of progress
795 and priorities. *Global Change Biology*, 24(1), 35–54. <https://doi.org/10.1111/gcb.13910>
- 796 Franco, M., & Silvertown, J. (1996). Life History Variation in Plants: An Exploration of the
797 Fast-Slow Continuum Hypothesis. *Philosophical Transactions of the Royal Society of*
798 *London B: Biological Sciences*, 351(1345), 1341–1348.
799 <https://doi.org/10.1098/rstb.1996.0117>
- 800 Friedlingstein, P., Cox, P., Betts, R., Bopp, L., von Bloh, W., Brovkin, V., et al. (2006). Climate-
801 carbon cycle feedback analysis: Results from the C4MIP model intercomparison. *Journal*
802 *of Climate*, 19(14), 3337–3353.
- 803 Friedlingstein, Pierre, Meinshausen, M., Arora, V. K., Jones, C. D., Anav, A., Liddicoat, S. K.,
804 & Knutti, R. (2014). Uncertainties in CMIP5 Climate Projections due to Carbon Cycle
805 Feedbacks. *Journal of Climate*, 27(2), 511–526. [https://doi.org/10.1175/JCLI-D-12-](https://doi.org/10.1175/JCLI-D-12-00579.1)
806 00579.1
- 807 Gelman, A., & Rubin, D. B. (1992). Inference from Iterative Simulation Using Multiple
808 Sequences. *Statistical Science*, 7(4), 457–472.
- 809 Janzen, D. H. (1970). Herbivores and the number of tree species in tropical forests. *American*
810 *Naturalist*, 104, 501–528.
- 811 Keenan, T. f., Baker, I., Barr, A., Ciais, P., Davis, K., Dietze, M., et al. (2012). Terrestrial
812 biosphere model performance for inter-annual variability of land-atmosphere CO2
813 exchange. *Global Change Biology*, 18(6), 1971–1987. [https://doi.org/10.1111/j.1365-](https://doi.org/10.1111/j.1365-2486.2012.02678.x)
814 2486.2012.02678.x
- 815 Kellndorfer, J., Walker, J., LaPoint, E., Bishop, J., Cormier, T., Fiske, G., et al. (2012). NACP
816 Aboveground Biomass and Carbon Baseline Data (NBCD 2000), U.S.A., 2000. Data set.
817 Available on-line at <http://daac.ornl.gov> from ORNL DAAC, Oak Ridge, Tennessee,
818 U.S.A. <http://dx.doi.org/10.3334/ORNLDAAC/1081>.
- 819 Knutti, R., Stocker, T. F., Joos, F., & Plattner, G. K. (2002). Constraints on radiative forcing and
820 future climate change from observations and climate model ensembles. *Nature*,
821 416(6882), 719–723.
- 822 LeBauer, D. S., Wang, D., Richter, K. T., Davidson, C. C., & Dietze, M. C. (2013). Facilitating
823 feedbacks between field measurements and ecosystem models. *Ecological Monographs*,
824 83(2), 133–154. <https://doi.org/10.1890/12-0137.1>
- 825 LeBauer, D. S., Dietze, M. C., & Bolker, B. M. (2014). Translating Probability Density
826 Functions: From R to BUGS and Back Again. *The R Journal*, 5, 1, pp. 207–209.

- 827 Leuning, R. (1995). A critical appraisal of a combined stomatal-photosynthesis model for C3
828 plants. *Plant, Cell & Environment*, 18(4), 339–355. <https://doi.org/10.1111/j.1365-3040.1995.tb00370.x>
- 830 Levin, S. A., Grenfell, B., Hastings, A., & Perelson, A. S. (1997). Mathematical and
831 Computational Challenges in Population Biology and Ecosystems Science. *Science*,
832 275(5298), 334–343. <https://doi.org/10.1126/science.275.5298.334>
- 833 Lin, J. C., Pejam, M. R., Chan, E., Wofsy, S. C., Gottlieb, E. W., Margolis, H. A., &
834 McCaughey, J. H. (2011). Attributing uncertainties in simulated biospheric carbon fluxes
835 to different error sources. *Global Biogeochemical Cycles*, 25(2), GB2018.
836 <https://doi.org/10.1029/2010GB003884>
- 837 Liu, F., Mladenoff, D. J., Keuler, N. S., & Moore, L. S. (2011). Broadscale variability in tree
838 data of the historical Public Land Survey and its consequences for ecological studies.
839 *Ecological Monographs*, 81(2), 259–275. <https://doi.org/10.1890/10-0232.1>
- 840 Mantooth, J. (2017). Tree Radial Growth and Carbohydrate Storage in Eastern US Temperate
841 Forest. PhD Dissertation. Department of Earth & Environment, Boston University.
- 842 Medvigy, D., Wofsy, S. C., Munger, J. W., Hollinger, D. Y., & Moorcroft, P., R. (2009).
843 Mechanistic scaling of ecosystem function and dynamics in space and time: Ecosystem
844 Demography model version 2. *Journal of Geophysical Research-Biogeosciences*, 114,
845 G01002, doi:10.1029/2008JG000812.
- 846 Medvigy, David. (2006). The state of the regional carbon cycle: Results from a coupled
847 constrained ecosystem-atmosphere model, Ph.D. thesis, Harvard University, Cambridge,
848 Massachusetts.
- 849 Medvigy, David, & Moorcroft, P. R. (2012). Predicting ecosystem dynamics at regional scales:
850 an evaluation of a terrestrial biosphere model for the forests of northeastern North
851 America. *Philosophical Transactions of the Royal Society of London B: Biological
852 Sciences*, 367(1586), 222–235. <https://doi.org/10.1098/rstb.2011.0253>
- 853 Moorcroft, P. R., Hurtt, G. C., & Pacala, S. W. (2001). A Method for Scaling Vegetation
854 Dynamics: The Ecosystem Demography Model (ed). *Ecological Monographs*, 71(4),
855 557–586. [https://doi.org/10.1890/0012-9615\(2001\)071\[0557:AMFSVD\]2.0.CO;2](https://doi.org/10.1890/0012-9615(2001)071[0557:AMFSVD]2.0.CO;2)
- 856 Pacala, S. W., & Deutschman, D. H. (1995). Details That Matter: The Spatial Distribution of
857 Individual Trees Maintains Forest Ecosystem Function. *Oikos*, 74(3), 357–365.
858 <https://doi.org/10.2307/3545980>
- 859 Parton, W., Stewart, J., & Cole, C. (1988). Dynamics of C, N, P And S in Grassland Soils - A
860 Model. *Biogeochemistry*, 5, 109–131.
- 861 Penning de Vries, F., Brunsting, A., & Van Laar, H. (1974). Products, requirements and
862 efficiency of biosynthesis: a quantitative approach. *Journal of Theoretical Biology*, 45,
863 339–377.

- 864 Plummer, M. (2010). JAGS (Just Another Gibbs Sampler). Version 2.2.0 user manual.
865 [http://ftp.jaist.ac.jp/pub/sourceforge/m/project/mc/mcmc-](http://ftp.jaist.ac.jp/pub/sourceforge/m/project/mc/mcmc-jags/Manuals/2.x/jags_user_manual.pdf)
866 [jags/Manuals/2.x/jags_user_manual.pdf](http://ftp.jaist.ac.jp/pub/sourceforge/m/project/mc/mcmc-jags/Manuals/2.x/jags_user_manual.pdf).
- 867 Raczka, B. M., Davis, K. J., Huntzinger, D., Neilson, R. P., Poulter, B., Richardson, A. D., et al.
868 (2013). Evaluation of continental carbon cycle simulations with North American flux
869 tower observations. *Ecological Monographs*, 83(4), 531–556. [https://doi.org/10.1890/12-](https://doi.org/10.1890/12-0893.1)
870 [0893.1](https://doi.org/10.1890/12-0893.1)
- 871 Ricciuto, D. M., Butler, M. P., Davis, K. J., Cook, B. D., Bakwin, P. S., Andrews, A., & Teclaw,
872 R. M. (2008). Causes of interannual variability in ecosystem-atmosphere CO₂ exchange
873 in a northern Wisconsin forest using a Bayesian model calibration. *Agricultural and*
874 *Forest Meteorology*, 148(2), 309–327, doi:10.1016/j.agrformet.2007.08.007.
- 875 Ricciuto, D. M., Schaefer, K., Thornton, P. E., Davis, K. J., Cook, R. B., Liu, S., et al. (2013).
876 NACP Site: Terrestrial Biosphere Model and Aggregated Flux Data in Standard Format.
877 Data set. Available on-line [<http://daac.ornl.gov><<http://daac.ornl.gov/>>] from Oak Ridge
878 National Laboratory Distributed Active Archive Center, Oak Ridge, Tennessee, USA.
879 <http://dx.doi.org/10.3334/ORNLDAAAC/1183>.
- 880 Ricciuto, Daniel M., King, A. W., Dragoni, D., & Post, W. M. (2011). Parameter and prediction
881 uncertainty in an optimized terrestrial carbon cycle model: Effects of constraining
882 variables and data record length. *Journal of Geophysical Research: Biogeosciences*,
883 116(G1), G01033. <https://doi.org/10.1029/2010JG001400>
- 884 Richardson, A. D., Williams, M., Hollinger, D. Y., Moore, D. J. P., Dail, D. B., Davidson, E. A.,
885 et al. (2010). Estimating parameters of a forest ecosystem C model with measurements of
886 stocks and fluxes as joint constraints. *Oecologia*, 164(1), 25–40.
- 887 Rogers, A., Medlyn, B. E., Dukes, J. S., Bonan, G., von Caemmerer, S., Dietze, M. C., et al.
888 (2017). A roadmap for improving the representation of photosynthesis in Earth system
889 models. *New Phytologist*, 213(1), 22–42. <https://doi.org/10.1111/nph.14283>
- 890 Saltelli, A., Ratto, M., Andres, T., Campolongo, F., Cariboni, J., Gatelli, D., et al. (2008).
891 *Global Sensitivity Analysis, The Primer*. John Wiley & Sons, Inc.
- 892 Schimel, D., Pavlick, R., Fisher, J. B., Asner, G. P., Saatchi, S., Townsend, P., et al. (2015).
893 Observing terrestrial ecosystems and the carbon cycle from space. *Global Change*
894 *Biology*, 21(5), 1762–1776. <https://doi.org/10.1111/gcb.12822>
- 895 Schupp, E. W., & Jordano, P. (2011). The full path of Janzen-Connell effects: genetic tracking of
896 seeds to adult plant recruitment. *Molecular Ecology*, 20(19), 3953–3955.
897 <https://doi.org/10.1111/j.1365-294X.2011.05202.x>
- 898 Schwalm, C. R., Williams, C. A., Schaefer, K., Anderson, R., Arain, M. A., Baker, I., et al.
899 (2010). A model-data intercomparison of CO₂ exchange across North America: Results
900 from the North American Carbon Program site synthesis. *Journal of Geophysical*
901 *Research: Biogeosciences*, 115(G3), G00H05. <https://doi.org/10.1029/2009JG001229>

- 902 Shiklomanov, A. (2018). *Improving Ecological Forecasts Using Data and Model Constraints*.
903 *PhD Dissertation*. Department of Earth & Environment, Boston University, Boston,
904 Massachusetts.
- 905 Shugart, H. H., Asner, G. P., Fischer, R., Huth, A., Knapp, N., Le Toan, T., & Shuman, J. K.
906 (2015). Computer and remote-sensing infrastructure to enhance large-scale testing of
907 individual-based forest models. *Frontiers in Ecology and the Environment*, 13(9), 503–
908 511. <https://doi.org/10.1890/140327>
- 909 Singsaas, E. L., Ort, D. R., & DeLucia, E. H. (2001). Variation in Measured Values of
910 Photosynthetic Quantum Yield in Ecophysiological Studies. *Oecologia*, 128(1), 15–23.
- 911 Sperry, J. S., & Love, D. M. (2015). What plant hydraulics can tell us about responses to
912 climate-change droughts. *New Phytologist*, 207(1), 14–27.
913 <https://doi.org/10.1111/nph.13354>
- 914 Sriver, R., Urban, N., Olson, R., & Keller, K. (2012). Toward a physically plausible upper bound
915 of sea-level rise projections. *Climatic Change*, (115), 893–902.
916 <https://doi.org/10.1007/s10584-012-0610-6>
- 917 Tang, J., Bolstad, P. V., & Martin, J. G. (2009). Soil carbon fluxes and stocks in a Great Lakes
918 forest chronosequence. *Global Change Biology*, 15(1), 145–155.
919 <https://doi.org/10.1111/j.1365-2486.2008.01741.x>
- 920 Thoning, K. W., Tans, P. P., & Komhyr, W. D. (1989). Atmospheric carbon dioxide at Mauna
921 Loa Observatory 2. Analysis of the NOAA GMCC data, 1974-1985. *Journal of*
922 *Geophysical Research-Atmospheres*, 94(D6), 8549–8565.
- 923 Trugman, A. T., Fenton, N. J., Bergeron, Y., Xu, X., Welp, L. R., & Medvigy, D. (2016).
924 Climate, soil organic layer, and nitrogen jointly drive forest development after fire in the
925 North American boreal zone. *Journal of Advances in Modeling Earth Systems*, 8(3),
926 1180–1209. <https://doi.org/10.1002/2015MS000576>
- 927 Walko, R. L., Band, L. E., Baron, J., Kittel, T. G. F., Lammers, R., Lee, T. J., et al. (2000).
928 Coupled Atmosphere–Biophysics–Hydrology Models for Environmental Modeling.
929 *Journal of Applied Meteorology*, 39(6), 931–944. [https://doi.org/10.1175/1520-0450\(2000\)039<0931:CABHMF>2.0.CO;2](https://doi.org/10.1175/1520-0450(2000)039<0931:CABHMF>2.0.CO;2)
- 931 Wang, D., LeBauer, D., & Dietze, M. (2013). Predicting yields of short-rotation hybrid poplar
932 (*Populus* spp.) for the United States through model–data synthesis. *Ecological*
933 *Applications*, 23(4), 944–958. <https://doi.org/10.1890/12-0854.1>
- 934 Weiss, A., & Norman, J. M. (1985). Partitioning solar radiation into direct and diffuse, visible
935 and near-infrared components. *Agricultural and Forest Meteorology*, 34, 205–213.
- 936 Weng, E. S., & Luo, Y. Q. (2011). Relative information contributions of model vs. data to short-
937 and long-term forecasts of forest carbon dynamics. *Ecological Applications*, 21(5), 1490–
938 1505.

939 Woods, K. D. (2000). Dynamics in Late-Successional Hemlock–Hardwood Forests Over Three
940 Decades. *Ecology*, 81(1), 110–126. [https://doi.org/10.1890/0012-](https://doi.org/10.1890/0012-9658(2000)081[0110:DILSHH]2.0.CO;2)
941 [9658\(2000\)081\[0110:DILSHH\]2.0.CO;2](https://doi.org/10.1890/0012-9658(2000)081[0110:DILSHH]2.0.CO;2)

942 Xu, X., Medvigy, D., Powers, J. S., Becknell, J. M., & Guan, K. (2016). Diversity in plant
943 hydraulic traits explains seasonal and inter-annual variations of vegetation dynamics in
944 seasonally dry tropical forests. *New Phytologist*, 212(1), 80–95.
945 <https://doi.org/10.1111/nph.14009>

946

947 Table 1. List of median parameter values for all 3 plant functional types (PFTs) used within the simulation (Figure 2). These median parameter values
 948 are based on the full posterior parameter distribution estimated using a meta-analysis approach (see Section 2.5.1) that combines expert priors [Dietze,
 949 Serbin *et al.* 2014] and trait data (Table S1). The “*” indicates that the parameter median values received additional hand-tuning to gain a reasonable
 950 distribution of successional PFTs for near present day conditions.

Parameter Name	Description	Units	Early Hardwood	Mid Hardwood	Late Hardwood
<i>Mort2</i>	Carbon balance mortality	year ⁻¹	20/3.50*	20/7.00*	20.0
<i>Root turnover rate</i>	Rate of fine roots to litter pool	year ⁻¹	0.691	0.681	0.673
<i>Growth respiration factor</i>	Fraction of assimilated carbon to growth respiration	gC gC ⁻¹	0.351	0.351	0.351
<i>Stomatal slope</i>	Ball-Berry stomatal parameter	dimensionless	5.87	5.75	5.87
<i>Fineroot2leaf</i>	Ratio of carbon allocated to fine roots/leaves	gC gC ⁻¹	0.636	0.995	1.47
<i>R fract</i>	Storage carbon allocated to recruitment	gC gC ⁻¹	0.318	0.316	0.312
<i>Labile fract</i>	Litter carbon allocated to labile carbon pool	gC gC ⁻¹	0.79	0.79	0.49
<i>Water conductance</i>	Measure of soil moisture stress	m ² kg leaf ⁻¹	0.00496	0.00470	0.00474
<i>Mort3</i>	Density independent mortality	year ⁻¹	0.001	0.001	0.001
<i>Specific leaf area</i>	Leaf area per leaf mass	m ² kg leaf ⁻¹	13.66	14.32	16.6
<i>Leaf respiration rate</i>	Leaf maintenance respiration	umol CO ₂ m ⁻² s ⁻¹	1.32	0.50	1.97

<i>Quantum efficiency</i>	Rate at which radiation is converted to assimilated carbon	$\mu\text{mol CO}_2 (\mu\text{mol photon})^{-1}$	0.0577	0.0396	0.045/0.06*
<i>V_{cmax} (25^oC)</i>	Carboxylation rate of photosynthesis	$\mu\text{mol CO}_2 \text{ m}^{-2} \text{ s}^{-1}$	39.65	41.64	44.8
<i>Root_respiration rate</i>	Controls rate of fine root respiration	$\mu\text{mol CO}_2 \text{ kg}^{-1} \text{ s}^{-1}$	8.34	8.34	8.31
<i>Minimum height</i>	Minimum height for reproduction	meters	5.00	5.00	5.00

951 Table 2: Parameter distributions for the late hardwood PFT as shown in Figure 3 as used in
 952 the sensitivity analysis. The values ‘*a*’ and ‘*b*’ define the constants of the distribution function
 953 [LeBauer *et al.*, 2014] for each parameter used in the sensitivity analysis. The sample size
 954 (*N*) is the number of mean trait observations used in the meta-analysis. Where trait data was
 955 not available the parameter distributions were defined as the prior (Figure 3). The 95%
 956 credible interval (lower bound, upper bound) for each parameter is provided. The parameter
 957 units are provided in Table 1.

Parameters	Distribution (a,b)	a	b	N	Median	Lower Bound	Upper Bound
<i>Mort2</i>	Gamma	1.47	0.0578	-	20.0	1.75	82.3
<i>Root turnover rate</i>	Weibull	1.55	0.862	-	0.49	0.053	0.94
<i>Growth respiration factor</i>	Beta	4.06	7.20	-	0.351	0.12	0.65
<i>Stomatal slope</i>	Lognormal	1.76	0.38	-	5.84	2.73	12.4
<i>Fineroot2leaf</i>	Gamma	8.75	7.89	2	1.47	0.412	2.52
<i>R fract</i>	Beta	2.00	3.00	-	0.312	0.046	0.72
<i>Labile fract</i>	Beta	1.50	1.50	-	0.49	0.053	0.94
<i>Water conductance</i>	Log normal	-5.40	3.00	-	0.00474	1.2e-05	2.17
<i>Mort3</i>	Uniform	0.00	0.02	-	0.001	5.1e-04	0.02
<i>Specific leaf area</i>	Normal	16.6	2.24	88	16.6	10.3	22.8
<i>Leaf respiration rate</i>	Weibull	2.72	1.86	44	1.97	0.33	3.61
<i>Quantum efficiency</i>	Gamma	4.46	59.7	13	0.06	0.02	0.22
<i>V_{max} (25°C)</i>	Normal	44.8	15.2	22	44.8	2.48	87.1
<i>Root respiration rate</i>	Weibull	2.00	10.00	-	8.31	1.37	19.3
<i>Minimum height</i>	Gamma	1.50	0.20	-	5.00	0.48	24.8

958

959 Table 3: Top parameter contributors to uncertainty based upon partial variance analysis for
 960 net primary productivity (NPP;<10 year). *Dietze, Serbin et al.* [2014] values are based upon
 961 the average contribution across all hardwood PFT sites.

Raczka NPP, (posterior w/ random effects)	Raczka NPP, (posterior, no random effects)	[<i>Dietze, Serbin et al.</i> 2014] NPP (posterior, no random effects)
<i>Quantum efficiency</i> (50%)	<i>Water conductance</i> (>50%)	<i>Growth respiration</i> (>50%)
<i>Leaf respiration rate</i> (25%)	<i>Growth respiration</i> (28%)	<i>Water conductance</i> (11%)
<i>Water conductance</i> (12%)	<i>Stomatal slope</i> (5%)	<i>Stomatal slope</i> (10%)
<i>Growth respiration</i> (12%)	<i>Mort2</i> (3%)	<i>Quantum efficiency</i> (7%)
		<i>Mort2</i> (6%)

962
 963
 964

 965

 966

 967

 968

 969

 970

 971

 972

 973

 974

 975

 976

977 Table 4: Top parameter contributors to uncertainty based upon partial variance analysis for
 978 above ground biomass (AGB;<10 year). The PFT type is variable across this comparison
 979 where Raczka=late hardwood PFT, Wang=poplar only (no random effects),
 980 LeBauer=switchgrass only (no random effects)

981

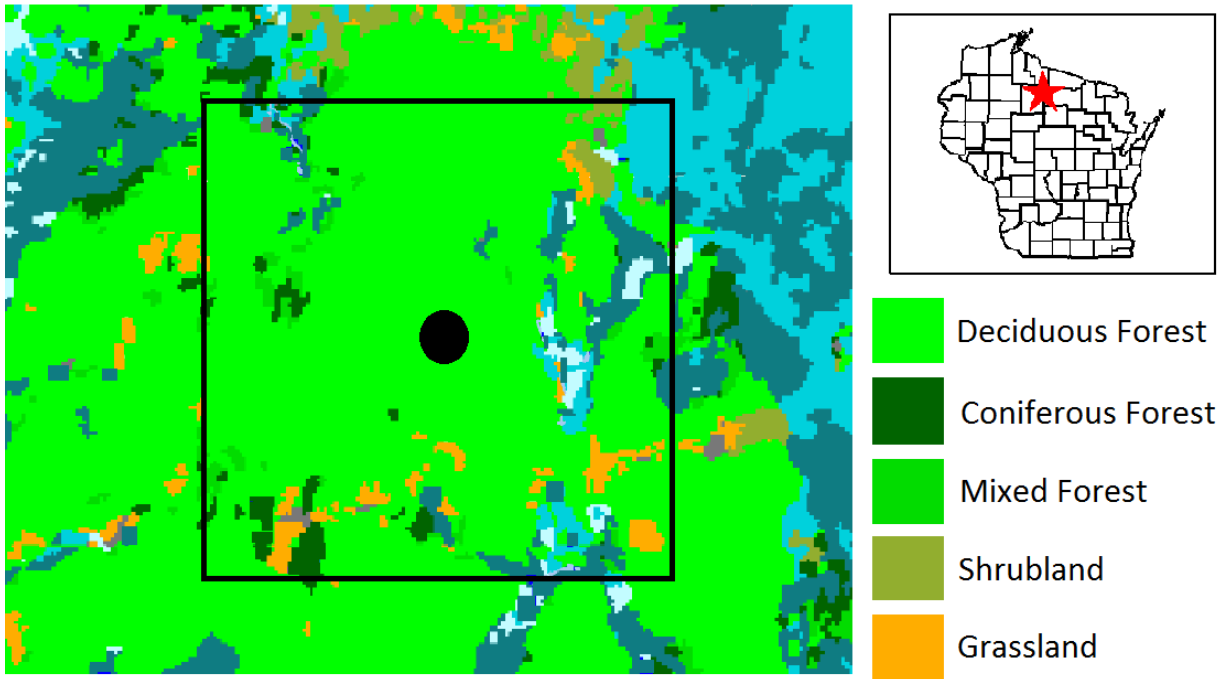
Raczka AGB, (posterior w/ random effects)	Raczka AGB, (posterior, no random effects)	[Wang et al. 2013] AGB, (poplar)	[LeBauer et al. 2013], AGB (switchgrass)	982 983 984
<i>Quantum effic.</i> (40%)	<i>Growth resp.</i> (>50%)	<i>Growth resp.</i>	<i>Growth resp.</i> (12%)	985
<i>Leaf resp. rate</i> (25%)	<i>Water cond.</i> (28%)	<i>Leaf resp.</i>	<i>fineroot2leaf</i> (10%)	986
<i>Water cond.</i> (15%)	<i>Minimum height</i> (23%)	<i>Quantum effic.</i>	<i>Leaf turnover</i> (7%)	987
<i>Growth resp.</i> (10%)	<i>Rep. alloc.</i> (5%)	<i>Mort2</i>	<i>SLA</i> (5%)	988
		<i>Water cond.</i>		989

990

991

992

993



994

995 Figure 1: Vegetation land cover map centered on the coordinates of Willow Creek, Wisconsin
 996 (latitude: 45.81, longitude: -90.08) indicated by the black dot. The black box represents the
 997 16 km² region from which the witness tree data observations were taken. This figure was
 998 created by data (ca. 2000) and plotting tools available at:
 999 <http://dnr.wi.gov/maps/gis/datalandcover.html>. All blue shades represent wetland.

1000

1001

1002

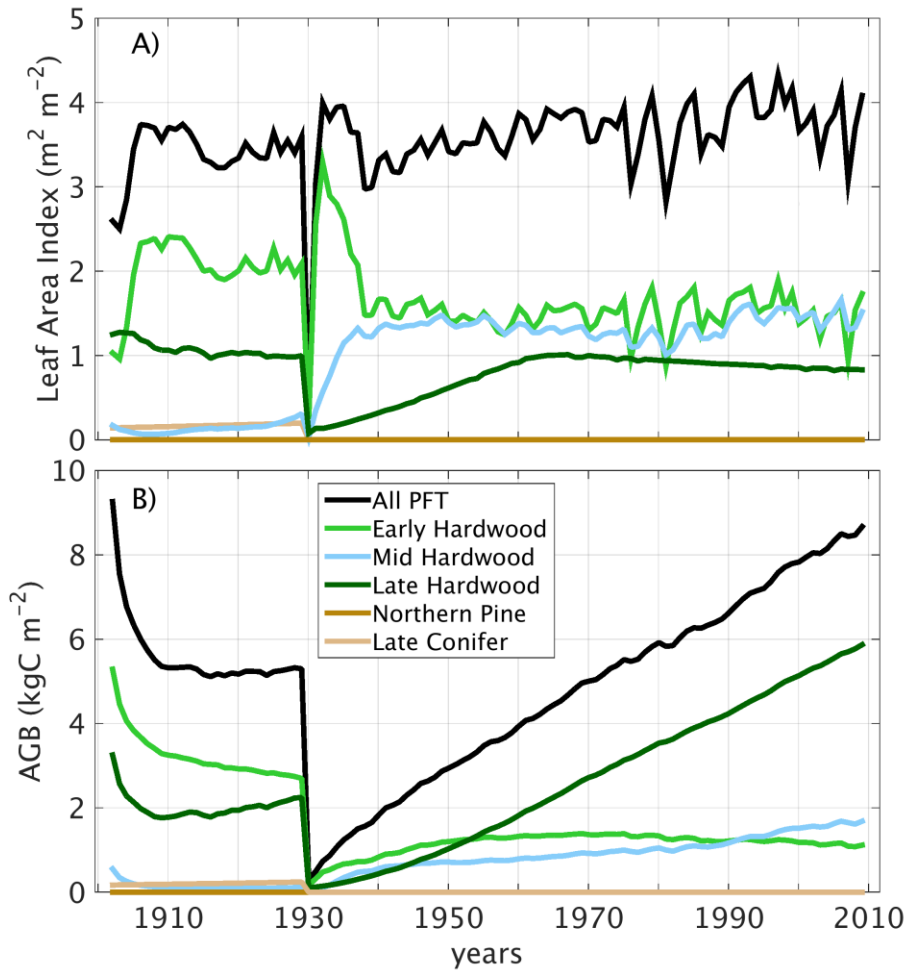
1003

1004

1005

1006

1007

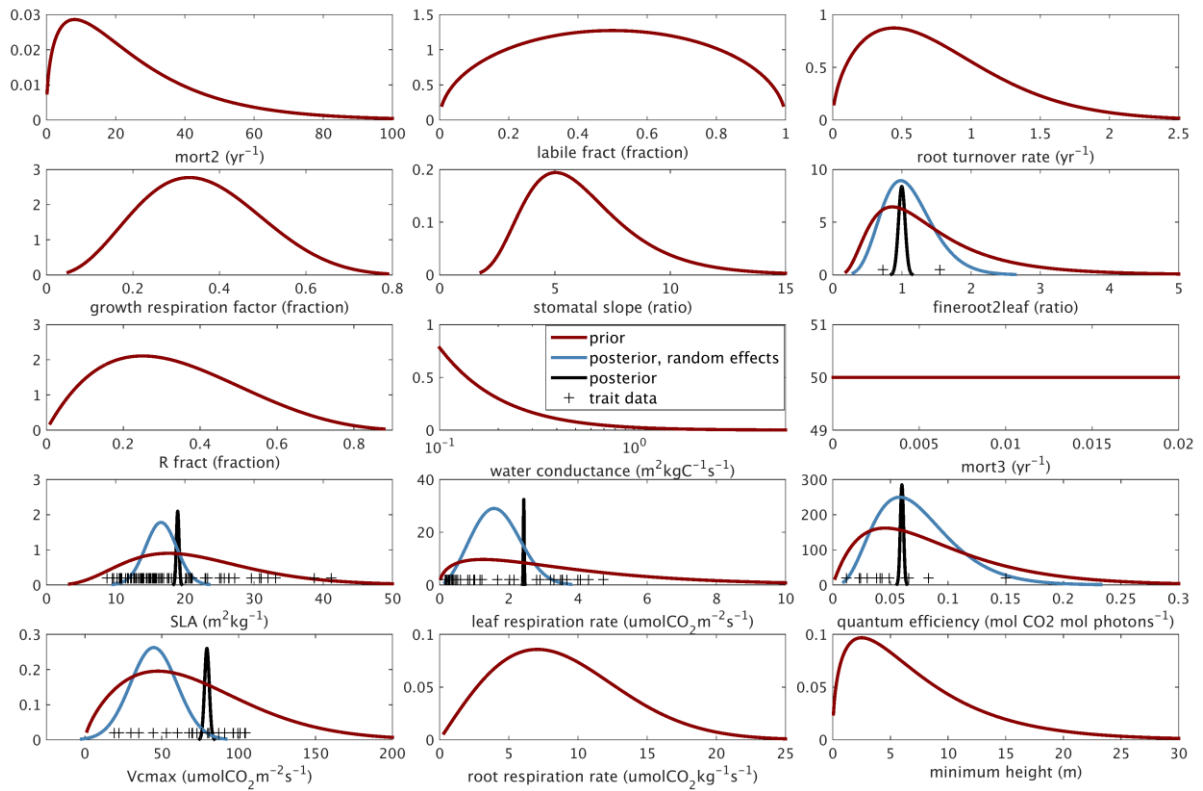


1008

1009 Figure 2: The simulation at Willow Creek (using the posterior median parameter values
 1010 provided in Table 1 of A) leaf area index and B) above-ground biomass (AGB). The sharp
 1011 drop at the year 1930 represents the logging event we prescribed upon the forest to mimic the
 1012 actual management history of this site.

1013

1014



1015

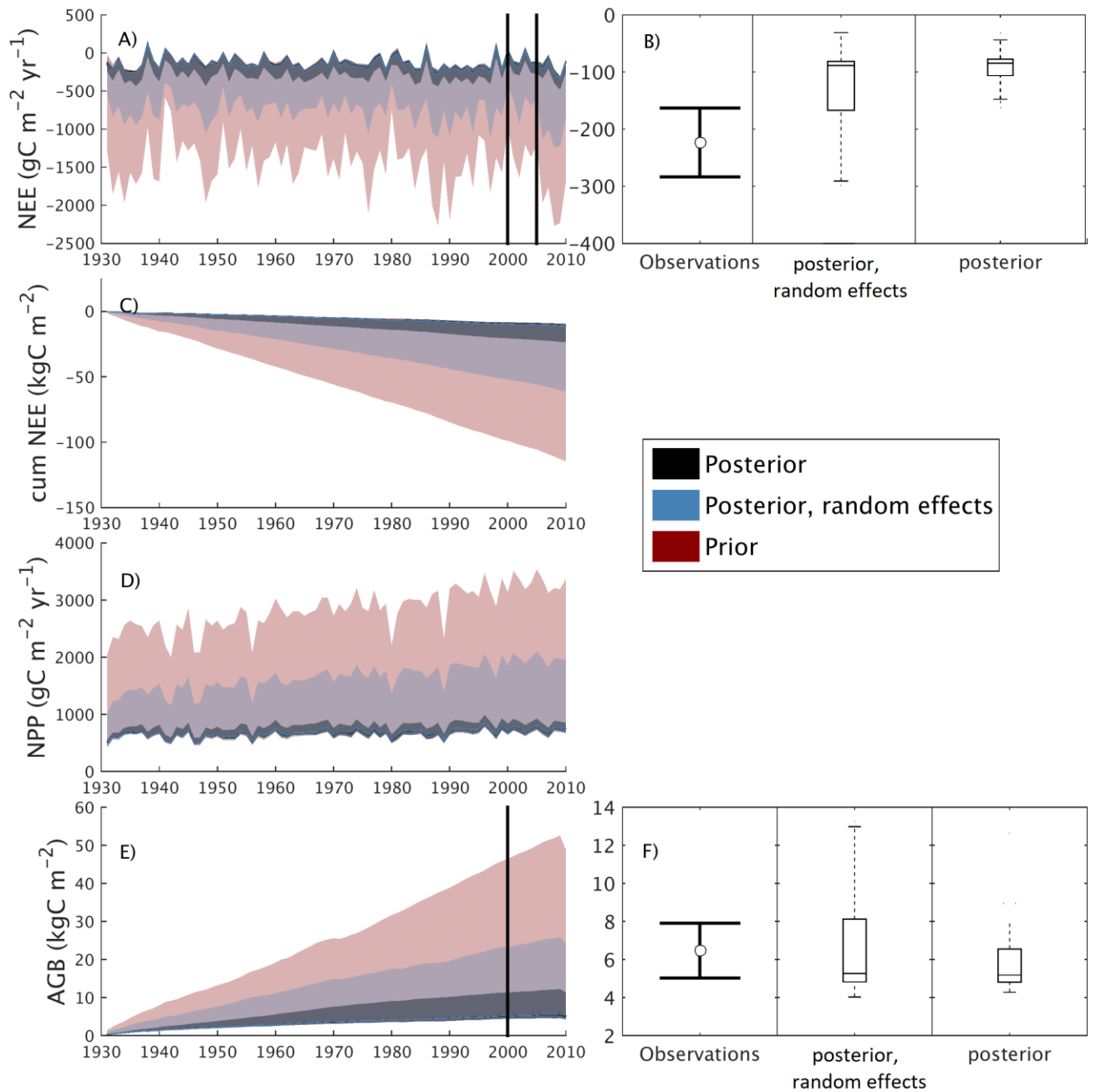
1016

1017

1018

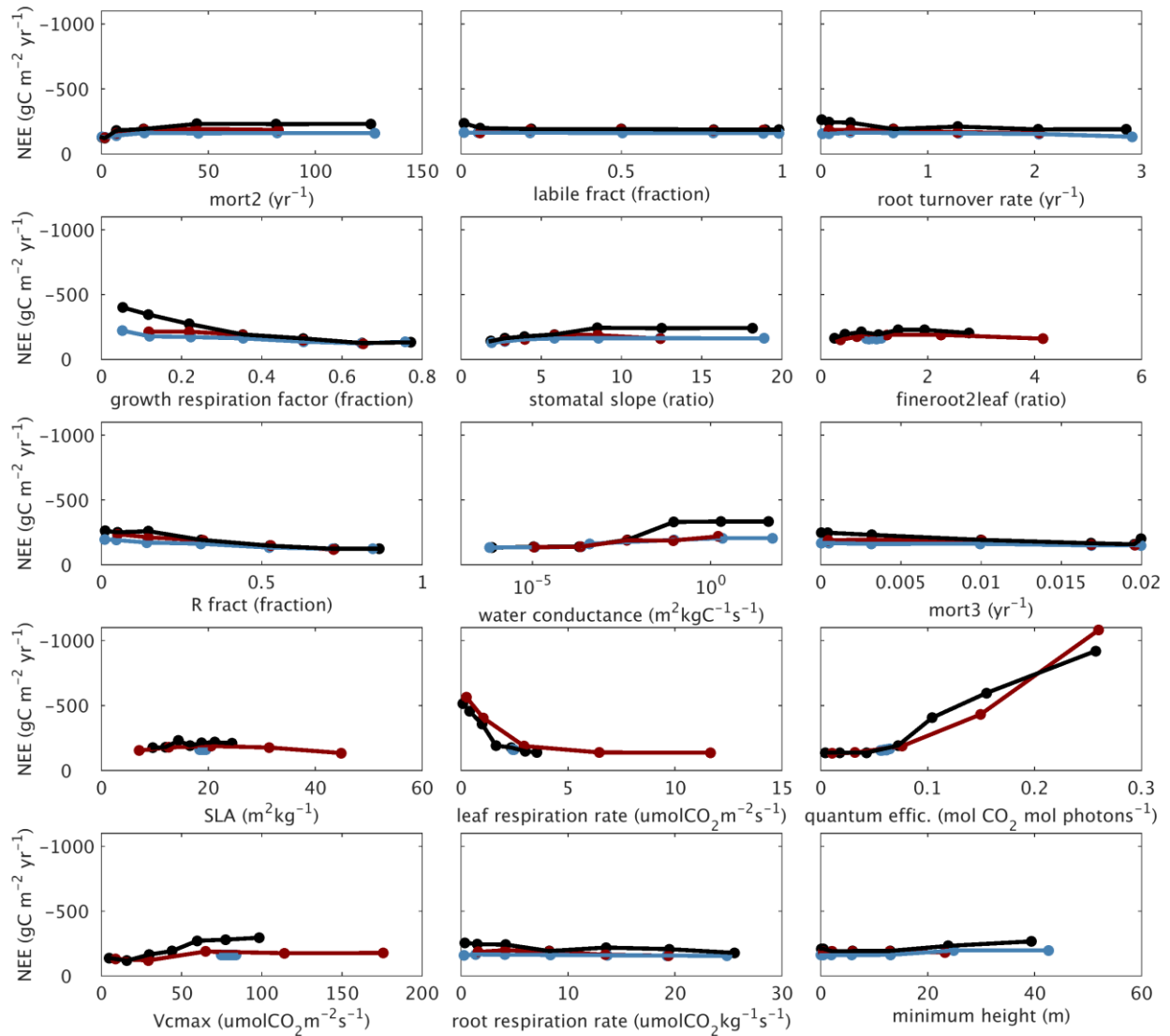
1019

Figure 3: Parameter distributions for the late successional plant functional type. The sensitivity analysis, variance decomposition and ensemble simulations were based off these distributions. Where trait data were available, a meta-analysis was performed to create posterior distributions.



1020

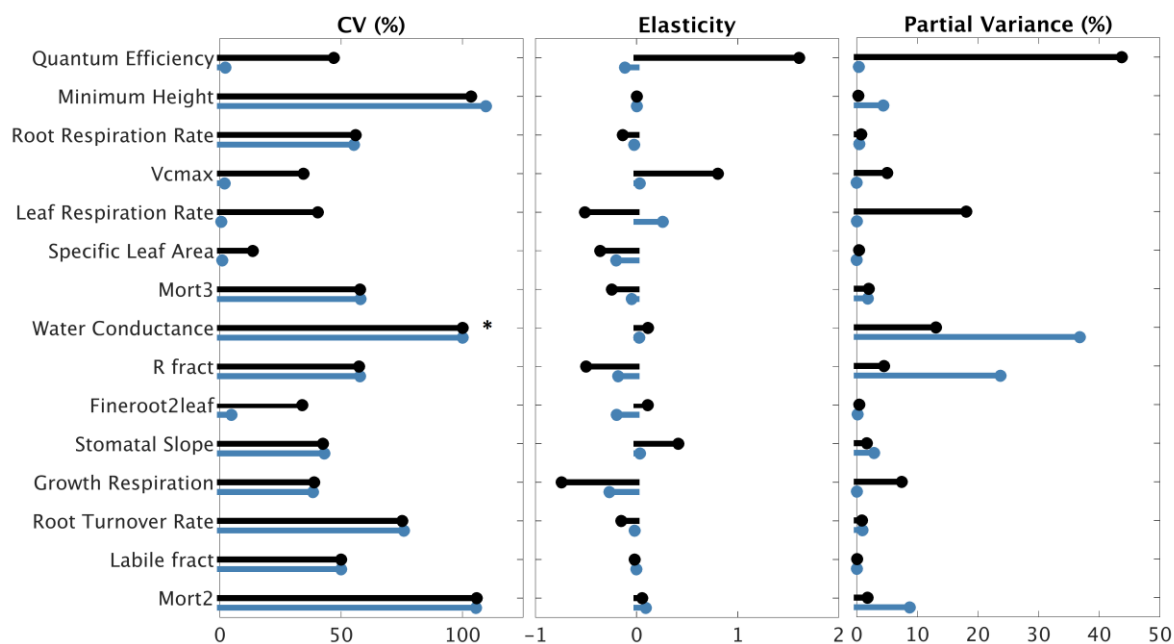
1021 Figure 4: The 95% confidence intervals (shaded region) for the model ensemble spread for
 1022 the prior, posterior with and without random effects parameter distributions for A) NEE, C)
 1023 cumulative NEE, D) NPP and E) AGB. Observations (panels B and F) are for the 2000-2005
 1024 mean NEE ($\pm 2\sigma$), and 2000 AGB ($\pm 2\sigma$). The model simulation ensemble spread for the
 1025 same time period respectively (vertical lines in panels A and E) is represented with box (25%,
 1026 median and 75% quartiles) and whisker (95% CI) plots (panels B and F). Negative NEE
 1027 values represent a carbon sink to the land.



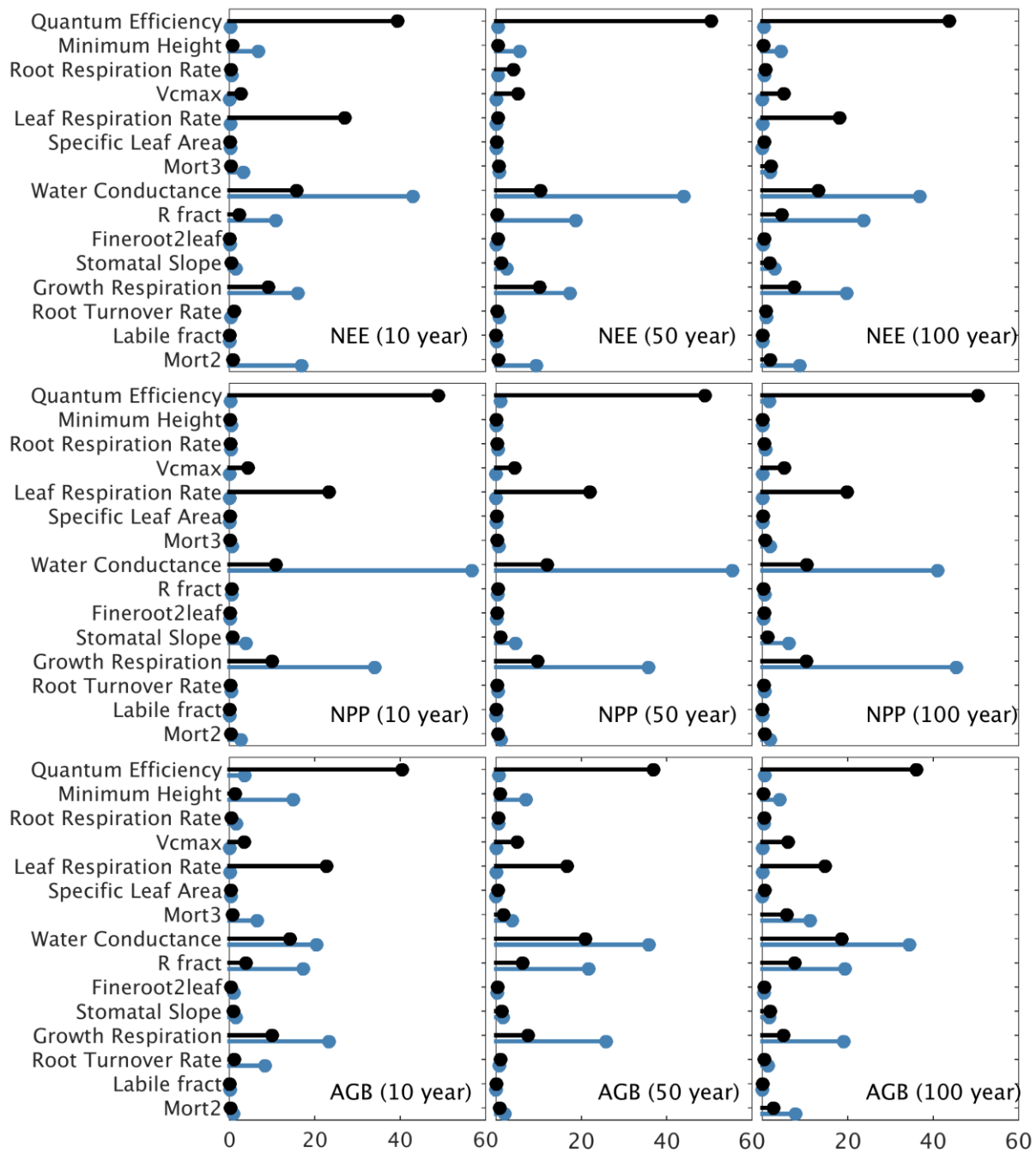
1028

1029 Figure 5: Sensitivity of simulated NEE (1935-2009 average; negative value=carbon sink) to
 1030 variation in parameters according to prior distribution (red), posterior distribution with
 1031 random effects (blue) and posterior distribution without random effects (black). The model
 1032 was evaluated at the median, $\pm 1, 2 \sigma$ quantiles for the prior distribution and the median, $\pm 1,$
 1033 $2, 3 \sigma$ quantiles for the posterior distributions. The evaluated model response is fitted with a
 1034 spline function for each parameter.

1035



1036
 1037 Figure 6: Contribution of parameters to centennial-scale model variance (1935-2009 average
 1038 NEE) for parameter uncertainty (coefficient of variation (CV), left panel), model sensitivity
 1039 (elasticity, middle panel), and model uncertainty (partial variance, right panel) for the
 1040 posterior distribution with random effects (blue) posterior distribution with no random effects
 1041 (black). The ‘*’ indicates that water conductance CV ($1.7 \times 10^6\%$) was displayed to 100 for
 1042 better viewing of all parameters.



1043

1044 Figure 7: The relative contribution of model uncertainty (partial variances) based on posterior
 1045 distribution with random effects (blue) and without random effects (black) for NEE, NPP and
 1046 AGB averaged for different time periods: 10yr = 1935-1940, 50 yr= 1935-1970, 100
 1047 yr=1935-2009.